Journal of South American Earth Sciences 119 (2022) 104045

Contents lists available at ScienceDirect

Journal of South American Earth Sciences

journal homepage: www.elsevier.com/locate/jsames

U-Pb geochronology of a reversely zoned pluton: Records of pre-to-post collisional magmatism of the Araçuaí belt (SE-Brazil)?

U.D. Bellon *, G.F. Souza Junior, F.A. Temporim, M.S. D'Agrella-Filho, R.I.F. Trindade

Institute of Astronomy, Geophysics and Atmospheric Sciences, Department of Geophysics, University of São Paulo, São Paulo, Brazil

ARTICLE INFO

Keywords:
Reversely zoned plutons
Post-collisional magmatism
Araçuaí Orogen
U-Pb geochronology
Venda Nova pluton

ABSTRACT

Post-collisional reversely zoned plutons occurring in the Araçuaí belt frequently show basic cores enveloped by felsic rocks, with intense magma mingling/mixing features. The Venda Nova (VN) pluton presents, in addition to its mafic core composed of gabbronorites surrounded by syenomonzonites, a narrow ring of charnockite and norite. The VN is considered as a marker of the last magmatic phases of the Araçuaí orogenic collapse and bears one of the few high-quality Cambrian paleomagnetic data for the West Gondwana, but no geochronological data is yet available for it. In this paper, we report new in-situ U-Pb geochronological data (SHRIMP II) for the syenomonzonite, gabbro and charnockite of the Venda Nova pluton. These data are discussed and compared to the geochemical and geochronological data available for the post-collisional magmatic rocks of the Araçuaí orogen. The concordant ages of the syenomonzonite (496.9 ± 4.2 Ma, MSWD = 0.0019, n = 14) and gabbro (500.6 ± 3.7 Ma, MSWD = 0.0290, n = 14) are likely the crystallization age of the main plutonic body and corroborate the previous interpretation of paleomagnetic data. In contrast, two age groups were identified for the charnockite: Group I (n = 14, 624.0 ± 3.1 Ma, MSWD = 0.116), which includes zircon borders and rims without evidence of border reaction, and Group II (n = 6, 483.7 ± 7.4 Ma, MSWD = 0.0003) from zircon grains with luminous rims and older cores. Since the Venda Nova charnockite has (i) a distinct geochemical signature compared to other post-collisional charnockite bodies found in the same region, (ii) higher magnetic anisotropy degrees compared to other border units of the same intrusion, and (iii) marked sub-solidus deformation features, the Group I ages are suggested as the crystallization age of these rocks, while Group II ages would be better interpreted as a resetting due to the thermal influence of the syenomonzonite and gabbro intrusions. This implies that the VN is a composite magmatic complex with contributions of magmas from the pre-collisional magmatic arc and from the post-collisional melts originated in the crust and mantle across the Araçuaí lithosphere during orogen collapse.

1. Introduction

The Neoproterozoic Araçuaí orogen (AO) has an extensive magmatic history (630-480 Ma, Pedrosa-Soares et al., 2011; Tedeschi et al., 2016). Around 530-480 Ma (Wiedemann et al., 2002), the tectonic regime changed from collisional to extensional, triggering voluminous amounts of post-collisional intrusions with various rock types. These intrusions occurred in a crustal relaxation zone parallel to the orogen metamorphic core, which was contemporaneously followed by the rise of melts originated in the mantle. In southern AO, rounded plutons exhibit reverse zoning (also referred as inversely zoned), where mantle-derived basic cores are enveloped by crustal melts, with extensive mixing/mingling features between them (Wiedemann et al., 2002; De Campos et al., 2004, 2016).

These reversely zoned plutons are still a theme of debate, since the mechanisms that generate them are not entirely understood yet. Recent studies using gravity data (Souza Junior et al., 2021) in one of these post-collisional reversely zoned plutons in the AO showed a well-defined distribution of mafic rocks in depth, which are surrounded by rocks formed from hybridization with the felsic envelope (the coeval post-collisional acid magmas). The mechanisms summoned to explain the formation of these plutons is mostly considered as coeval diapiric ascent of mafic and felsic magmas through deep conduits (Bayer et al., 1987; Wiedemann et al., 2002; De Campos et al., 2004, 2016; Temporim et al., 2020; Bellon et al., 2021; Souza Junior et al., 2021).

One of the interesting features of the post-collisional intrusions of the

* Corresponding author.
E-mail address: ualisson.bellon@usp.br (U.D. Bellon).

https://doi.org/10.1016/j.jsames.2022.104045
Received 28 March 2022; Received in revised form 10 September 2022; Accepted 20 September 2022
Available online 26 September 2022

AO is the Venda Nova pluton (VN). This reversely zoned pluton mainly includes a gabbroic core and a syenomonzonitic envelope externally associated to microcline-granites and leucogranites (which are a probable result of melting of the paragneisses, one of their country rocks, during igneous emplacement, Ludka et al., 1998), but in addition to this archetypal inverse structure the VN has an outer ring of charnockite and norite (Mendes and De Campos, 2012). The VN has been studied over two decades in terms of its geochemical features (Horn and Weber-Diefenbach, 1987; Ludka et al., 1998; Mendes and De Campos, 2012; De Campos et al., 2016), and more recently with focus on the magnetic fabric to enhance the understanding of their emplacement mechanisms and tectonostructural control (Bellon et al., 2021). High quality paleomagnetic data have also been acquired from the syenomonzonite, gabbro and charnockite which resulted in a key Cambrian pole (VN pole) for West Gondwana (Temporim et al., 2021). Mendes and De Campos (2012) argued that charnockites from the outer ring of the pluton are geochemically distinct from other charnockitic post-collisional rocks of AO, and were not derived from the same magma that originated the gabbroic core. Anisotropy of magnetic susceptibility studies also show that charnockites present anomalously high anisotropy degrees, even when compared with other portions of the VN borders (Bellon et al., 2021). These authors have proposed that charnockitic rocks in VN were most likely a previous pulse, in which the syenomonzonites and gabbros were later intruded.

So far, every interpretation of VN as part of the post-collisional history of the AO is based on indirect evidence, namely its rounded shape, the internal arrangement of its igneous facies and the fact that the host rocks main fabric is deflected by the pluton. In this paper, we analyze U-Pb geochronological data (sensitive high-resolution ion microprobe, SHRIMP-II) in zircons extracted from gabbros, syenomonzonites and charnockites from the VN pluton. These results were then discussed and compared with geochronological data of other Cambro-Ordovician plutons of the AO.

2. Geological setting and previous results

2.1. The Araçuaí orogen (AO)

The Ribeira, Araçuaí and Western Congo belts form an orogenic system, ~500 km wide and >1000 km long, resulting from the final amalgamation of West Gondwana in the Neoproterozoic to early Paleozoic times (Fig. 1) (Pedrosa-Soares et al., 2001; Alkmim et al., 2006). This Neoproterozoic-Cambrian orogen is contained in a great recess delineated on three sides by ancient, crystalline basement rocks of the São Francisco and Congo cratons. The Araçuaí orogen merges to the south with the coastal Ribeira orogen, forming the Araçuaí-Ribeira orogenic system (AROS) (Tedeschi et al., 2016; Egydio-Silva et al., 2018).

The AO has been interpreted in two ways. A collisional-subduction model, involving the creation of a lithospheric oceanic basin covered by the Adamastor ocean during the Tonian taphrogenesis, which produced a cratonic bridge connecting the paleo continents of Africa (Congo Craton) and South America (São Francisco Craton) (Alkmim et al., 2006). Alternatively, geothermal data, structural analysis and quantitative modeling have been integrated to suggest an intracontinental setting for the development of the AO (Fossen et al., 2017, 2020; Cavalcante et al., 2018, 2019; Konopásek et al., 2020). More recently, Caxito et al. (2022) have summarized a series of multiproxy

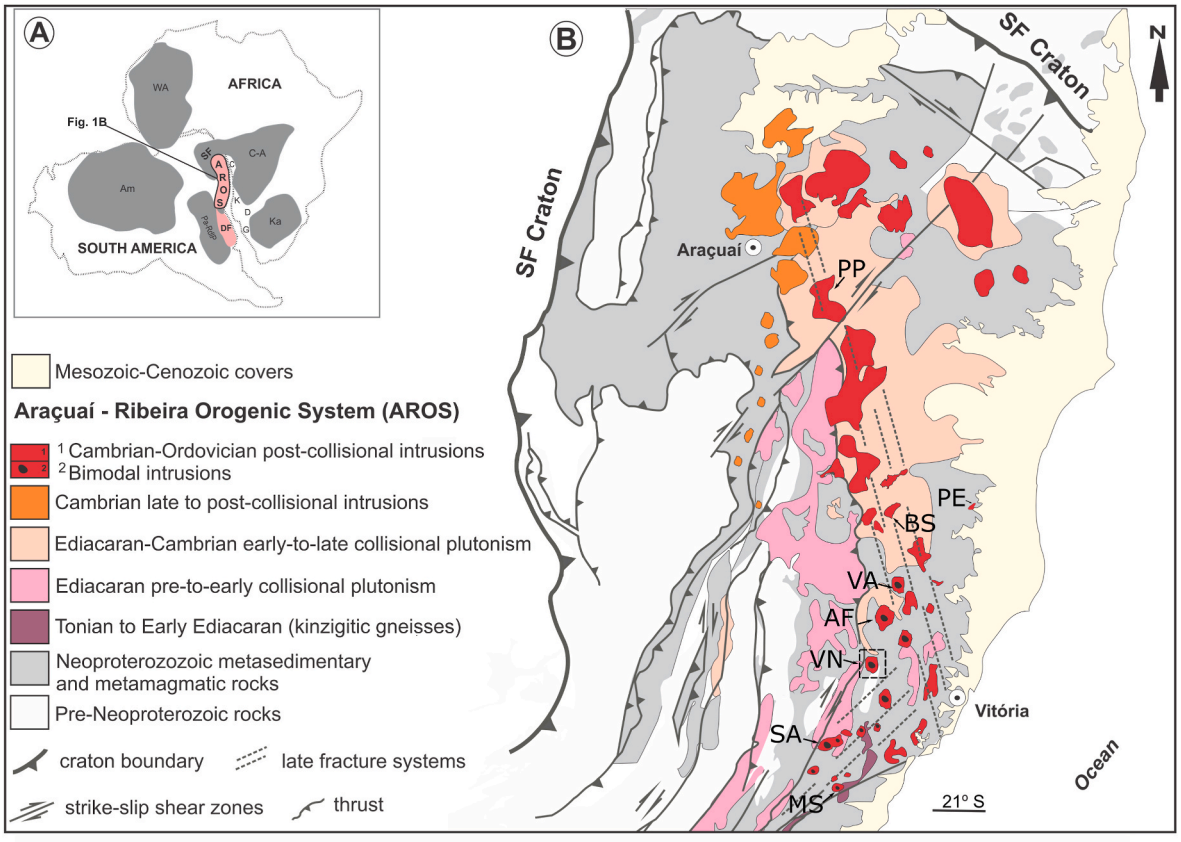

Fig. 1. (A): Spatial position of the Araçuaí-Ribeira orogenic system (AROS) together with the Dom Feliciano (DF) orogenic system in a pre-rift configuration, based on Alkmim et al. (2006) and De Campos et al. (2016). Cratons are represented in dark gray by: Am- Amazon, SF - São Francisco, Pa-RdlP - Paranapanema, Luiz Alves and Rio de la Plata, Ka - Kalahari, Wa - West African, C-A - Congo-Angola. (B): Araçuaí orogen (AO), with emphasis on the Cambrian-Ordovician intrusions: Venda Nova (VN), Afonso Claudio (AF), Barra do São Francisco (BS), Mimoso do Sul (MS), Pedra do Elefante (PE), Padre Paraíso (PP), Santa Angélica (SA) and Várzea Alegre (VA).

evidences to support a complete Wilson Cycle history, supporting the consumption of the Adamastor oceanic lithosphere and, lately, a continental collision and final amalgamation of the Gondwana continent. Anyhow, both models accommodate the intense magmatic activity observed in the AO with ages between 630 and 480 Ma which implies a high-temperature regime sustained for ~90 m.y. in the orogen core, followed by a significant decrease in magmatic-metamorphic activity (ca. 540–520 Ma) before the post-collisional igneous episode (Pedrosa-Soares et al., 2020). Numerous studies have been published during the last decades, mainly on the petrology, geochronology, and geochemistry of the Araçuaí belt magmatism (Bayer et al., 1987; Horn and Weber-Diefenbach, 1987; Ludka et al., 1998; Medeiros et al., 2000; Wiedemann et al., 2002; De Campos et al., 2004; Mendes et al., 2005; Pedrosa-soares et al., 2007; Mendes and De Campos, 2012; Tedeschi et al., 2016; Peixoto et al., 2017; Serrano et al., 2018; Cristina Araujo et al., 2020; Temporim et al., 2020). Based on these data, Pedrosa-Soares et al. (2020) grouped the different plutonic rocks from AO into five supersuites that follow the typical geochemical and structural evolution of collisional settings and range in age from the early Ediacaran to the Cambrian-Ordovician times (630–480 Ma): pre-collisional G1 (630–580 Ma), syn-collisional G2 (585–545 Ma), late collisional G3 (545–530 Ma), post-collisional G4 (530–500 Ma) and G5 (500–480 Ma).

The northern post-collisional bodies have intruded in shallower crystallization pressures in the range of 2.4–3.5 kbar (phase equilibrium modeling on garnet-cordierite neosome furnished P-T, Serrano et al., 2018). Post-collisional rocks of south Araçuaí were emplaced at pressures around 5.7–11.5 kbar (geobarometric calculations using Al-contents in amphiboles, Wiedemann et al., 2002). The current exposure levels represent crustal sections from former depths of ~10 km in the north to ~30 km in the south (Wiedemann et al., 2002; Serrano et al., 2018). In the northern section of the AO, they form large, elongated N-striking bodies subparallel to the belt. Amalgamated intrusions include granitic batholiths with only subordinate mafic components (Serrano et al., 2018). Isotopic studies carried in post-collisional

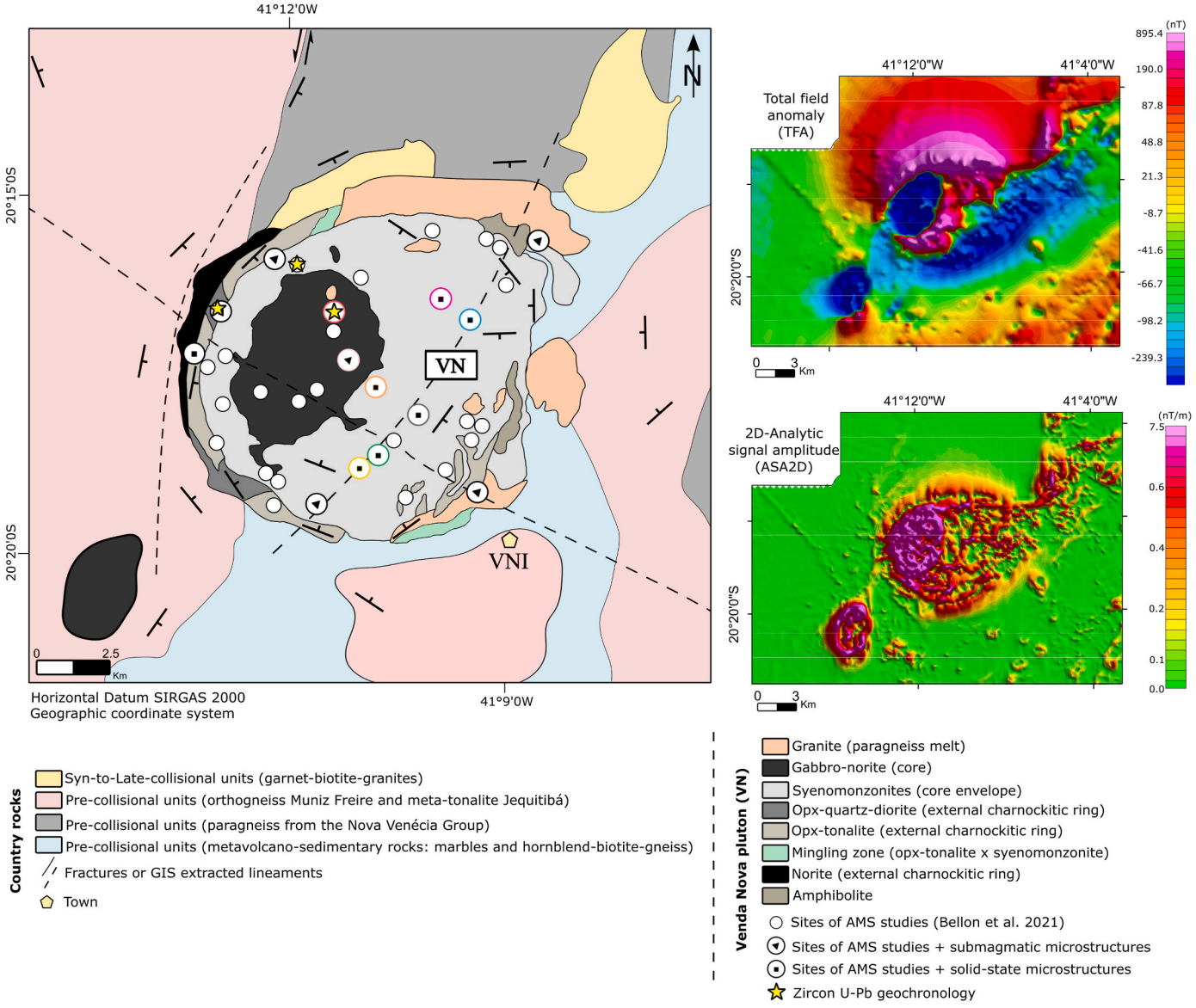

Fig. 2. (A): Geological map of the Venda Nova pluton (modified from Bellon et al., 2021 after Mendes and De Campos, 2012). Yellow stars indicate sample location for zircon U-Pb geochronological analyses. VNI: Venda Nova do Imigrante city, Espírito Santo, Brazil. (B): the limits of the Venda Nova from aeromagnetic products, Total field anomaly (TFA) and 2D-Analytic signal amplitude (ASA2D) highlighting the rounded shape of the intrusion and its segmentation from the country rocks. Aeromagnetic maps were obtained after gridded data from the Espírito Santo Aerogeophysical Survey (1093) (CPRM, 2010); flight lines have a spacing of 500 m in the N-S direction and 10 km in the E-W direction, with a flight height of 100 ± 15 m above the ground.

charnockite-granite associations in the northern section of AO have shown that granites and charnockites have distinct Lu-Hf signatures, evidencing distinct crustal sources for magmas in a same geological formation (Melo et al., 2020). In contrast, in the south the volume of post-collisional magma is significantly lower, the intrusions are smaller, circular or elliptical in shape with concentric magnetic fabrics (Temporim et al., 2020; Bellon et al., 2021). These plutons comprise mainly I-type and A-type granitic rocks, and their charnockitic equivalents (similar opx-bearing lithotypes) (Pedrosa-Soares and Wiedemann-Leonardos, 2000; De Campos et al., 2004, 2016). In this sector of the orogen, post-collisional intrusions usually form reversely-zoned balloon-like plutons, composed of granitic-charnockitic borders and gabbronoritic cores, with striking magma mixing and mingling features, with chemical-isotopic evidence of mantle involvement in their genesis (De Campos et al., 2004, 2016).

2.2. Geology of the Venda Nova (VN) pluton

The Venda Nova (VN) is a rounded reversely zoned pluton with an area of almost 75 km^2 (Fig. 2). It intrudes pre-collisional orthogneisses and paragneisses (migmatitic Al-rich rocks whose main protolith were gray wacky sediments, ranging from biotite-free cordierite-bearing granulites to biotite-rich gneisses - Gradim et al., 2014) which are cut by NE-trending dextral transpressive shear zones (Wiedemann et al., 2002 and references therein). The foliation of the country rocks deflects and envelopes the VN units with subvertical contacts, but tends to return to the regional NE-SW trend far from the pluton borders (Bellon et al., 2021). Besides submagmatic features, the VN borders also show evidence of plastic and dynamic deformation around the elliptical intrusion of the syenomonzonite envelope of the pluton, which is a common feature observed in other post-collisional plutons (Wiedemann et al., 2002). Souza Junior et al. (2021) have suggested that this effect could be explained by the dragging of country rocks as a result of the diapiric granite intrusion (ductile downward flow of the country rocks that causes foliations of high angle dips), or in the case where the volume of mafic material is high enough due to an inverse diapiric process caused by the sinking of the denser mafic core, which may increase solid-state deformational features at the borders of the pluton.

The main geological units of the VN are (Ludka et al., 1998): (i) a gabbro-norite core with local olivine-pyroxene-phlogopite cumulates, (ii) a syenomonzonitic envelope and (iii) an intermediate monzodiorite halo between the mafic core and the syenomonzonitic rocks, resulting from the mixing of these magmas. Probably the most interesting feature of the VN pluton is a narrow charnockitic/noritic ring at its western border. Mendes and De Campos (2012) have performed a detailed investigation on the geochemical features of these charnockitic rocks (which will be discussed later in the next section of this paper). When comparing the gabbros of VN core, which are enriched in Ba, Zr, Sr and LREE and originated from an enriched alkaline primitive parental magma (Ludka et al., 1998), Mendes and De Campos (2012) argued it would not be possible to produce the medium-K calc-alkaline charnockites not enriched in incompatible elements. Lastly, granites also appear at the VN borders, which have been interpreted as resulting from the partial melting of the country rocks (paragneisses from the Nova Venécia group, Ludka et al., 1998).

This structure (VN) appears clearly on aeromagnetic maps (Fig. 2). The total field anomaly (TFA) shows an intense anomaly in the VN borders and a reverse anomaly in the center of the pluton coinciding with the mafic core. The 2D-Analytic signal amplitude (ASA2D) delineates the contacts between the internal facies of VN and also the contact between the pluton and the country rocks. The mafic core is highlighted by strong internal gradients, but the gradient associated with the charnockitic ring is not different from that of the country rocks. Interestingly, 2 km southwest of VN there is an elliptic anomaly similar to that of the VN gabbroic core, that shows a well-defined border in the ASA2D. This intrusion could be a satellite body of the VN emplaced along the same structure (Ludka and Wiedemann-Leonardos, 2000).

Gabbro-norites from the mafic core were described by Ludka et al. (1998) as composed of labradorite, diopside, orthopyroxene, hornblende (with accessory phases of by biotite, magnetite and sulphides) with local occurrences of olivine-pyroxene-phlogopite cumulates. Magmatic features include intergranular interstitial texture where the space between plagioclase laths is filled with pyroxene (mostly hypersthene) and biotite (Bellon et al., 2021). The syenomonzonitic rocks (from the felsic envelope) are composed of microperthitic microcline (or mesoperthite), oligoclase/andesine with minor amounts of biotite, quartz and other accessory phases such as zircon, titanite, apatite and magnetite (Ludka et al., 1998). Local occurrences of monzodiorites show mantling of feldspars and pyroxene-amphibole transformations (Ludka et al., 1998), interpreted as signs of chemical imbalance due to non-homogeneous mixing of gabbro-norites and syenomonzonites.

According to Mendes and De Campos (2012) the narrow western charnockitic ring is segmented into two units, a more external noritic layer and a charnockite layer, towards the internal part of the intrusion. The norite has an intergranular to hypidiomorphic granular texture, composed of labradorite to anorthite, orthopyroxene and clinopyroxene, hornblende (mainly as overgrowing pyroxenes), magnetite and other accessory phases (including zircon). The charnockite is usually porphyritic, also composed of andesine, orthopyroxene and clinopyroxene, amphibole and biotite (locally isolated as euhedral crystals), k-feldspar, quartz, and other phases like magnetite and zircon, ranging from opx-tonalite to opx-granodiorite.

2.3. Geochemical data of VN and other post-collisional intrusions of the AO

In Fig. 3 we present geochemical data compiled from the literature for the VN and similar post-collisional units, including basic rocks (<52% of SiO_2 wt%), syenites, monzonites and other high-K cal-alkaline/alkaline rocks, as well as charnockitic rocks (Wiedemann et al., 1986, 2002; Horn and Weber-Diefenbach, 1987; Mendes et al., 1997, 2005; Ludka et al., 1998; Mello, 2000; Medeiros et al., 2001; De Campos et al., 2004; Pedrosa-Soares et al., 2006; Baltazar et al., 2010; Novo et al., 2010; Mendes and De Campos, 2012; Gonçalves et al., 2014, 2016; Zanon et al., 2015; Aranda et al., 2020).

The gabbro-norite core of VN plot in both the tholeiitic as in the calc-alkaline field, together other post-collisional basic rocks from the AO (Fig. 3), but they naturally tend to be more calc-alkaline. Gabbro-norites from the VN pluton have a metaluminous signature, which is also coherent with other basic examples from the G5. There is a spreading from the alkali to the calcic series in the Frost et al. (2001) diagram also similar to other post-collisional basic rocks.

The high values of K_2O, together with $^{87}Sr/^{86}Sr$ ratios, of intermediary and basic rocks in most of the post-collisional rocks have been interpreted as a result of heterogeneous interaction of basic magmas with more felsic ones (granitic), suggesting a hybrid origin for them (De Campos et al., 2016). Syenomonzonites from the VN have essentially a calc-alkaline signature in the AFM diagram (Fig. 3). The signatures are, however, unclear in the molar A/NK vs. A/CNK diagram (Shand, 1927), with some samples falling in the peraluminous and peralkaline fields, even though most of the monzonites, syenites and high-K calk-alkaline/alkaline post-collisional rocks fall in the metaluminous field. Furthermore, syenomonzonites of the VN are in the alkali field of the Frost et al. (2001) diagram, whereas other post-collisional rocks lie between the alkali-calcic and calcic-alkali series.

Venda Nova charnockites are calc-alkaline, more magnesian than other post-collisional charnockites (Fig. 3), and outstandingly metaluminous (compared to other G5 charnockites) for a calcic series of rocks and less enriched in incompatible elements when compared to other post-collisional charnockites (Mendes and De Campos, 2012). They differ from G5 charnockites, such as Várzea Alegre and Padre Paraíso plutons (502.7 ± 1.9 Ma; Xavier, 2017), in some aspects, the

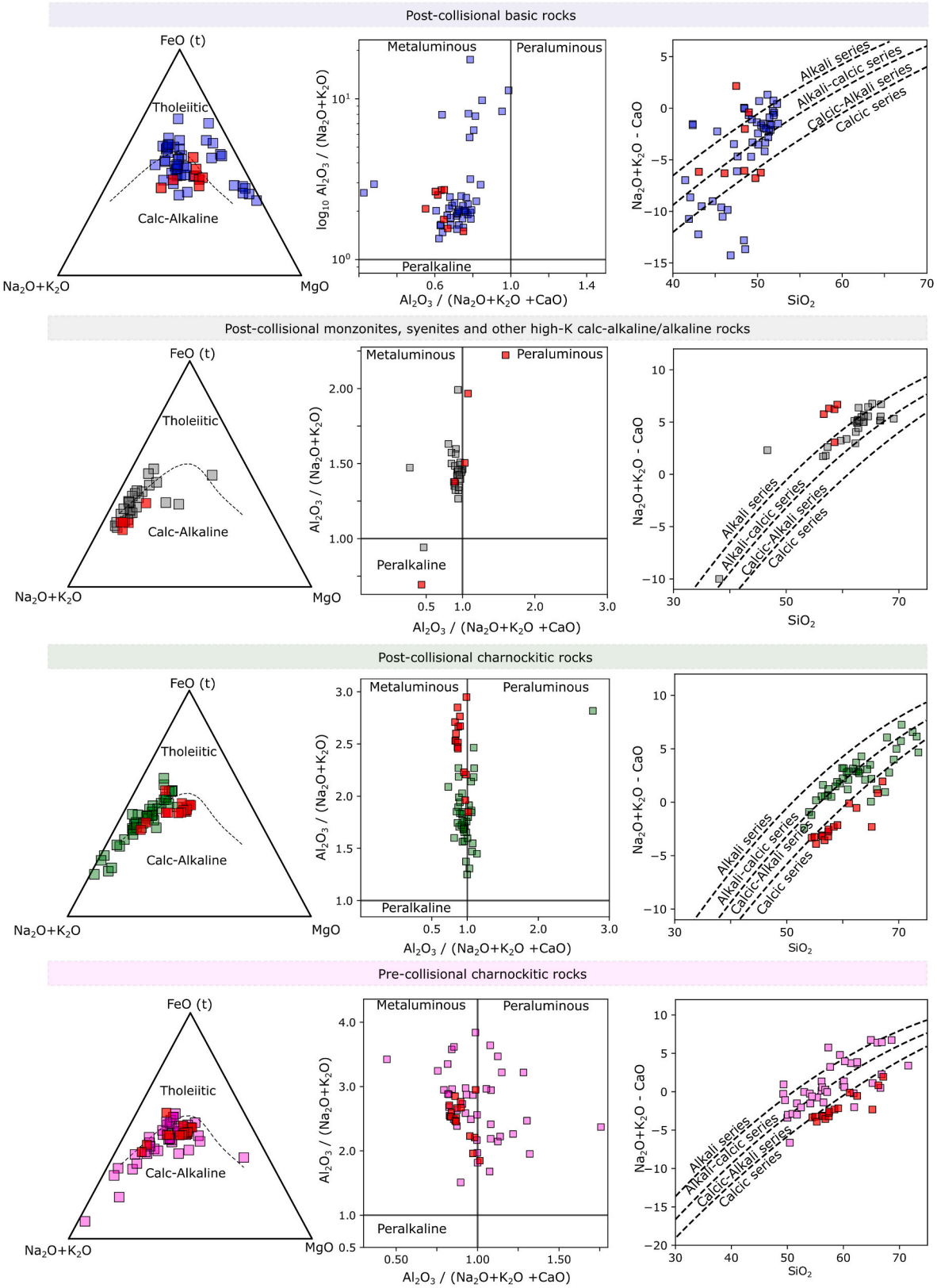

Fig. 3. Compilation of geochemical data for post-collisional (G5) basic rocks (<52% of SiO_2), post-collisional syenites/monzonites and other high-K calc-alkaline/alkaline rocks, as well as post-collisional (G5) and pre-collisional (G1) charnockitic rocks from the Araçuaí orogen. Data from Venda Nova is represented in red in all plots. From left to right: AFM diagram (Irvine and Baragar, 1971), A/NK vs. A/CNK diagram (molar) (Shand, 1927), and ($Na_2O + K_2O - CaO$) x SiO_2 (wt%) diagram showing series based in alkalis/calcic content (Frost et al., 2001) diagram. For post-collisional basic rocks, a $\log_{10}$ scale was used in the vertical axis to better represent all samples. Data compiled from: Wiedemann et al. (1986), 2002; Horn and Weber-Diefenbach (1987); Mendes et al. (1997), 2005; Ludka et al. (1998); Mello (2000); Medeiros et al. (2001); De Campos et al. (2004); Pedrosa-Soares et al. (2006); Baltazar et al. (2010); Novo et al. (2010); Mendes and De Campos (2012); Gonçalves et al. (2014), 2016; Zanon et al. (2015); Aranda et al. (2020).

post-collisional charnockitic rocks of the AO being more enriched in LILE and HFSE. Crystallization temperatures for VN charnockite, estimated from microprobe analysis in pyroxenes range from 915 ± 25 °C to 960 ± 50 °C, and re-equilibrium temperatures are around 600 ± 50 °C (Mendes and De Campos, 2012). Al-in-hornblende geobarometer of Schmidt (1992) (mineral association of the VN charnockites were exactly the same proposed in his paper), provides crystallization pressures around 5.5 ± 0.6 kbar (18–20 km depth), suggesting that these charnockites were emplaced at the root of plutonic structures (Mendes and De Campos, 2012). The paragenesis of VN charnockites points towards an anhydrous high-temperature genetic condition, but a minor amount of primary hornblende and biotite occurs in these rocks as well. However, as discussed by Mendes and De Campos (2012, and references cited therein), hornblende and biotite can crystalize under minor water content if K-availability is high enough. Data from seismology studies from Assumpção et al. (2013) shows a current continental crust of 40 km in depth in the southern portion of the AO, which suggests that these charnockites intruded in a thick crust of around 60 km of depth. Therefore, although the charnockites from VN are spatially restrict to a narrow ring in the western part of the pluton, most of its previous volume could have been removed through surface processes (denudation), which especially agrees with the interpretation of them being a root a plutonic structure.

We have also compared VN charnockites with pre-collisional (G1) charnockitic examples from northern AO formations: the Derribadinha tonalite, Suíte Divino and, lastly, Chaves pluton (Novo et al., 2010; Gonçalves et al., 2014; Tedeschi et al., 2016).

The Derribadinha Tonalite is a NS-elongated gneissic batholith (Gonçalves et al., 2014). It comprises a large amount of small, greenish, fine-to-medium grained enderbitic bodies. Charnockitic rocks (opx--bearing) are magnesian metaluminous rocks, going from the calcic to alkali-calcic series. These are enriched in LREE over HREE, and have $(La/Yb)_N$ ratios that goes from 4 up to 47, with both positive and negative Eu anomalies (Gonçalves et al., 2014). The geochronological data pointed to two crystallization ages of 580 ± 8 Ma (U-Pb, LA-ICPMS, Petitgirard et al., 2009) and 597 ± 4 Ma (U-Pb LA-ICPMS, Gonçalves et al., 2014). Meanwhile, zircon overgrowths constrain the age of the metamorphic event to around 561 ± 8 Ma (U-Pb SHIRIMP, Da Silva et al., 2011).

The Divino suite comprises an NNE-SSW elongated plutonic body of mafic to felsic charnockite, intruding the Juiz de Fora complex (Paleoproterozoic basement) during the AO's pre-collisional stage (U-Pb SHIRIMP ages of 592 ± 7 and 603 ± 4 Ma, Novo et al., 2010). These are mostly metaluminous potassium-rich rocks of an expanded calc-alkaline series, enriched in LILE, with acidic rocks showing more positive Eu anomalies while mafic rocks have negative ones. εNd values for the Divino rocks (≈-10) indicate an important crustal contribution (Novo et al., 2010). Geochemical and Nd isotopic signatures suggest that the Divino suite evolved in a continental magmatic-arc setting, being also interpreted as the granulitic root of this arc (Novo et al., 2010).

The Chaves pluton is a NS-elongated elliptical body composed mostly of enderbitic facies with minor charnockite, gabbronorite, opdalite and biotite monzogranite facies (Tedeschi et al., 2016). The contacts between those facies have transitional mixing features (hybrid zones). Crystallization ages are calculated as 599 ± 15 Ma (U-Pb, SHRIMP, Tedeschi et al., 2016). Geochemical data suggests strong magma contamination by the Paleoproterozoic basement. The enderbites follow mostly the alkali-calcic trend, being magnesian metaluminous rocks, with a major crustal component in their genesis ($^{87}Sr/^{86}Sr$ at 0.70682 and εNd varying from −4.9 to −6.8) (Tedeschi et al., 2016).

Charnockitic rocks from the VN are considerably more calcic and metaluminous than other post-collisional charnockites. But there is no clear evidence (through major geochemical elements) of their segregation from other post-collisional charnockites. We have compiled data of the lanthanides of syenites, monzonites and high-K calc-alkaline/alkaline rocks, gabbros and charnockites (both G1 and G5) and plotted it against VN samples. Unfortunately, there are few data for syeno-monzonites and gabbros from VN, but they follow other post-collisional rocks from the AO. Charnockitic lanthanide data is fortunately more abundant. From spidergrams (Fig. 4), one can notice that not only Venda Nova charnockites are less enriched in LREE and HREE than other post-collisional charnockites, but also less enriched than pre-collisional ones.

Also, VN charnockites have much lower contents of potassium (Fig. 5A) and barium than other post-collisional charnockites. El Bouseily and El Sokkary (1975) stated that considering the ternary relationship between Rb, Ba and Sr might be useful to follow differentiation trends in igneous suits. We have plotted data from the pre-collisional and post-collisional charnockitic rocks of the AO and compared them with VN charnockite data (Fig. 5).

As discussed in their work (El Bouseily and El Sokkary, 1975): (i) with increasing the acidity (silica content), Ba increases compared to Sr

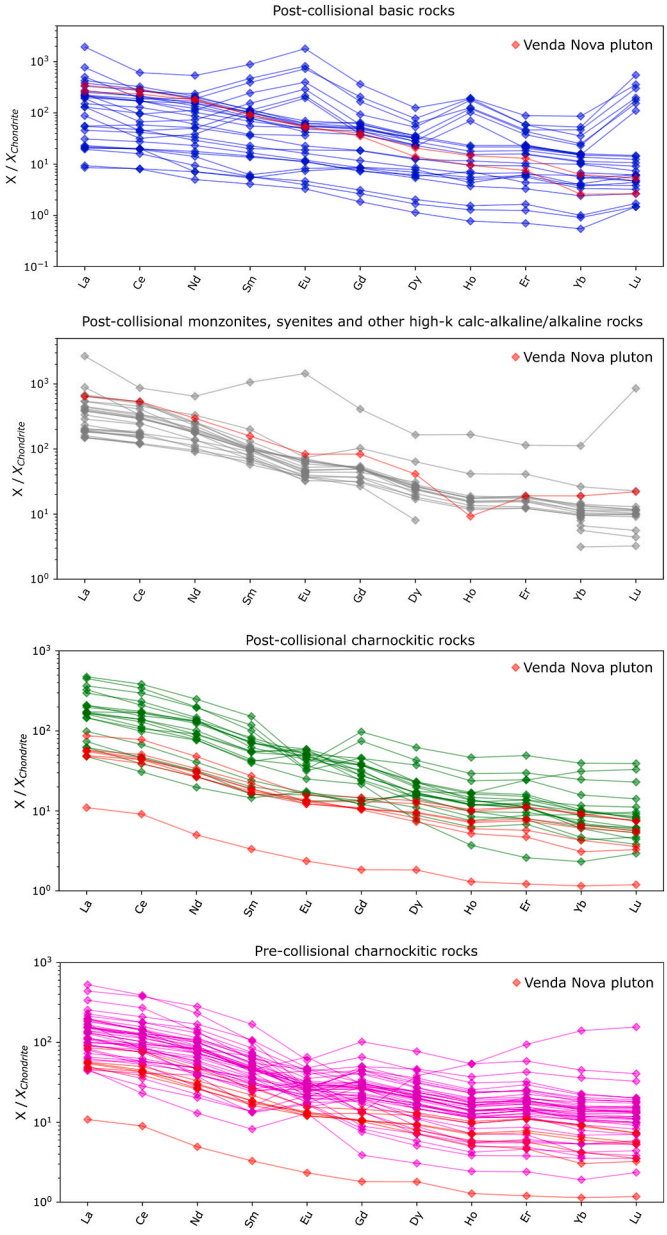

Fig. 4. Compiled data (spidergrams normalized by chrondrite: Boynton, 1983; Wakita et al., 1971) of post-collisional rocks (basic rocks, monzonites, syenites and other high-K calc-alkaline/alkaline rocks, and charnockites) and pre-collisional charnockites compared with VN data. Source of data is the same as those cited in Fig. 3.

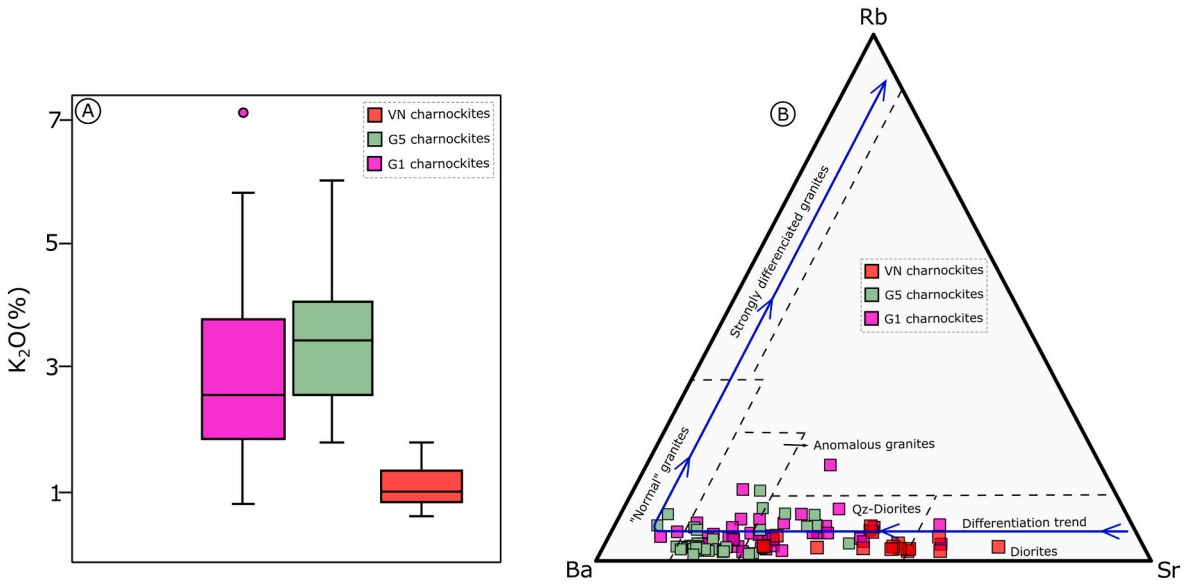

Fig. 5. (A): amount of K_2O in pre- and post-collisional charnockites of AO, in comparison with VN-charnockites. (B): Ternary relation between differentiation and Rb-Ba-Sr content (El Bouseily and El Sokkary, 1975). Differentiation trend is indicated by the blue line (and its arrows), which is marked by a decrease in Sr and concomitant increase in Ba, followed by an enrichment in Rb. VN charnockites seems to be less differentiated than other charnockites from the AO.

(while Rb does not suffer significant changes); (ii) Sr decreases as differentiation proceeds; (iii) "normal granites" are referred as low-Ca granitic rocks, which are strongly enriched in Ba; (iv) Rb/Ba values quickly increase in strongly differentiated granites, and; (v) anomalous granites (which include metassomatized and granitized rocks) are those considered to have relatively high Rb values, but still lower than "normal granites". Most of the post-collisional charnockites plot in the field of anomalous granites (Fig. 5), which could be related to the Rb-fractioning during magmatic processes and due to their high amount of Ba compared to Sr and Rb. Pre-collisional charnockites are spread between the less differentiated field towards the "normal granites". Venda Nova charnockites are the less enriched in Rb and also less enriched in Ba than most of the pre and post-collisional charnockites of the AO. Besides, the ternary relation between Rb-Ba-Sr indicates that charnockitic rocks from VN are less differentiated than G5 post-collisional rocks.

2.4. Magnetic fabric and anisotropic parameters

Magnetic fabric, depending on the geological history of the rock, is usually coherent with magmatic flow and magmatic foliation (Bouchez, 1997). AMS data can also be used to track paleostress, since the main susceptibilities are usually parallel to the deformation ellipsoid (k_1 being parallel to the X-axis and k_3 to the Z-axis) (Borradaile and Henry, 1997).

Bellon et al., (2021) focus their work on correlating microstructure and anisotropy of magnetic susceptibility data in order to understand the emplacement mechanism of the Venda Nova pluton and to study the strain field of the crust where its magmas have intruded. Here, we aim to discuss how AMS data, microstructures and geochronological data might enhance the interpretation of VN's geological history.

Bellon et al. (2021) performed AMS measurements in an Agico Kappabridge MFK 1A equipment, where all of the samples are individually measured to obtain, following Jelínek (1978), the eigenvalues of a second-rank symmetrical tensor (k_1, k_2 and k_3). Data from each of the specimens is used to form an ellipsoid of orthogonal susceptibility-axes, in which $k_1 > k_2 > k_3$, that when well constrained to magnetic mineralogy content can be related to preferential structures in rocks (Bouchez, 1997). Parameters (Table 1) related to these eigenvalues (often called main susceptibilities) are useful to evaluate the shape of each ellipsoid (specimen) and how anisotropic they can be. The anisotropy degree (P, Eq. (1)) quantifies the difference between the largest and smallest susceptibility-axes and, together with the shape parameter (T, Eq. (2)), it helps to understand how the magnetic fabric is structured. Negative T values imply prolate ellipsoids, while positive values indicate oblate ones (Jelinek, 1977, 1981; Jelínek, 1978).

Table 1
Parameters of anisotropy of magnetic susceptibility. From: Jelinek (1977, 1981) and Jelínek (1978).

Symbol	Equation
P (Eq. (1))	$\left(\frac{k_1}{k_3}\right)$
T (Eq. (2))	$\left(\frac{2 \bullet \ln(k_2) - \ln(k_1) - \ln(k_3)}{\ln(k_1) - \ln(k_3)}\right)$

Magnetic fabric data from anisotropy of magnetic susceptibility (AMS) revealed a concentric foliation pattern, coherent with a diapiric intrusion mainly controlled by buoyancy forces with minor influence of tectonic stress (Bellon et al., 2021). Similar to other post-collisional plutons from the southern portion of the AO, such as the Santa Angélica pluton (Temporim et al., 2020), the Venda Nova likely resulted from the gravitational collapse of the Araçuaí orogen. This mechanism is triggered by a change of a collisional to an extensional regime around 530-480 Ma, where a crustal relaxation zone parallel to AO metamorphic core induces partial decompressing melting of the asthenospheric mantle (Wiedemann et al., 2002; De Campos et al., 2016). Passive transport of magma through deep rheological week zones (shear zones and deep faults) in the AO leads to ascension of basic mantellic and felsic crustal magmas forming the diapiric reversely zoned plutons in the southern AO (Wiedemann et al., 2002; Pedrosa-soares et al., 2007; Bellon et al., 2021).

We gathered data from all of the samples measured by Bellon et al. (2021) and calculated a boxplot distribution of each unit (Fig. 6A). Magnetic mineralogy has already been investigated for these samples, that yield a normal fabric dominated by multidomain magnetite (Bellon et al., 2021). More than 75% of the samples from the syenomonzonites show P values smaller than 1.2. Higher values for this unit do exist, but statically they are outliers in a major and symmetric distribution, and are associated to the syenomonzonitic rocks at the borders of the pluton (where magma flow interacts with the country rocks) and to specific

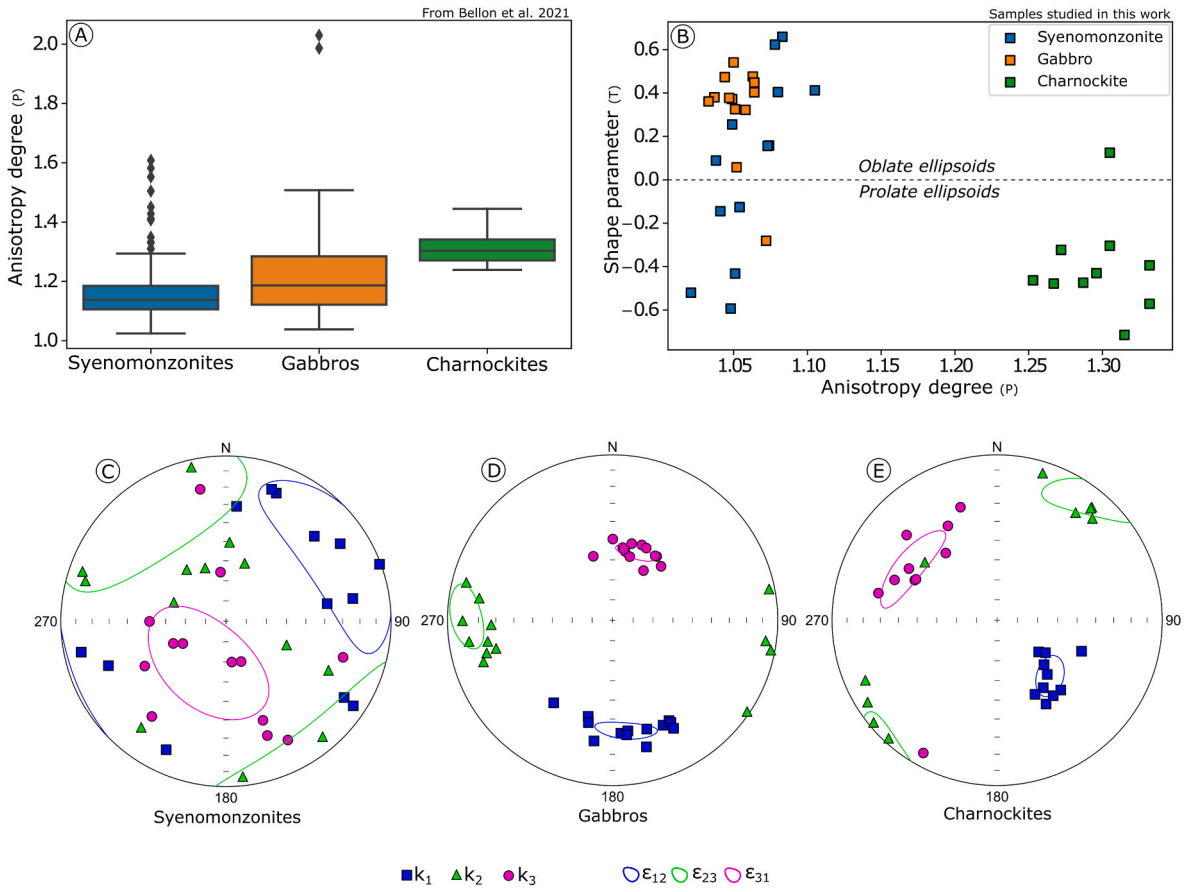

Fig. 6. Compiled magnetic information from Bellon et al., (2021). (A) Boxplots showing the distribution of the anisotropy degree (P) in the main facies of the VN pluton (all of the samples). Statistical outliers are represented by diamonds. (B) Anisotropy degree x shape parameter (T) of samples from the sites dated in this work. (C), (D) and (E) Stereograms showing the distribution of k_1, k_2 and k_3 (and its internal dispersion) from sites correspondent to samples dated in this work (syenomonzonite from VNU20, gabbronorite from VNU32 and an opx-tonalite from VNU8).

portions of the pluton (as indorsed by Bellon et al., 2021). Gabbroic rocks show the greatest span of *P* values, its distribution is asymmetric, but more than 75% of them are lower than 1.3. Although the distribution of *P*-values of charnockitic rocks is asymmetric, it yields the shortest boxplots (the median is very close first and third quartiles).

Specifically comparing the samples from the same sites (that we have dated in this work) in the Jelinek plot (Fig. 6B), the anisotropy degree of the charnockites is distinct from the syenomonzonites and gabbros. The shape parameter of the charnockites is essentially negative, indicating prolate ellipsoids, while the gabbro is positive (in the oblate ellipsoid field). The syenomonzonite, however, show a more disperse behavior along the T-axis, and shares the same range of anisotropy degree with the gabbro.

Although we do not aim to perform an analysis of the AMS directions (since it was already performed by Bellon et al., 2021), we show new AMS ellipsoids of samples from the same sites dated in this paper as well. $k_2$and k_3 is highly disperse for the syenomonzonites (VNU20, Fig. 6C), when compared with gabbros (VNU32, Fig. 6D), and charnockites (VNU8, Fig. 6D), which indicates a more isotropic behavior of the magnetic fabric, with no preferential orientation, even being close to border regions of the pluton. The gabbros, however, show an oblate magnetic fabric, most likely a result of the alignment of paramagnetic minerals (such as biotite and pyroxenes) in the magmatic fabric and very thin acicular inclusions (that includes opaques) along the greatest elongation axis.

Very often, directions determined through AMS studies are in fact the principal strain directions (Borradaile, 1991). Although the anisotropy degree is not restricted related to deformation, it indicates a magnetic fabric with more preferential alignment in the charnockites when compared to the other units in the pluton, which also agrees with macroscopic observation of dextral shearing in granitic/syenomonzonitic dykes in the charnockites (as reported by Bellon et al., 2021).

3. Methods

Samples from three distinct units of the VN pluton have been investigated here: a gabbro from the mafic core, a syenomonzonite and a charnockite (check Fig. 2 to see their spatial position). These samples belong to the same sites studied for anisotropy of magnetic susceptibility and paleomagnetism by Bellon et al. (2021) and Temporim et al. (2021): VNU32 (gabbro), VNU20 (syenomonzonite) and VNU8 (charnockite) (Fig. 2). These sites were chosen because they did not show any clear signs of chemical/physical magma interaction that could result in mixing of populations of zircons from different magmatic facies. Thin sections were also prepared from the same rocks chosen for geochronological investigation.

The zircon grains were separated in the Research Center in Geochronology and Isotopic Geochemistry (CPGeo) at the University of São Paulo. Samples were first superficially cleaned of weathered materials, crushed and then comminuted with a disc mill. Sequentially, the material was sieved and concentrated on a Wilfley stirring table. The magnetic fraction was then separated using first a hand neodymium magnet and then a Frantz magnetic separator at two electric currents (0.5 A and them 1.5 A). The nonmagnetic fraction passed through density separation with bromoform (2.89 g/cm^3) and methylene iodide

(3.32 g/cm^3) in order to obtain a concentrate of dense minerals. Zircons were manually handpicked from the final concentrate using a binocular microscope and mounted into discs of epoxy resin (2.5 cm in diameter). Discs were sanded and polished to expose a cross-section of the grains at the disc surface.

These zircon grains were studied in terms of their morphology and texture through transmitted and reflected light, and then gold plating to be imaged by cathodoluminescence (CL). These images were used to guide the spots. U-Pb analyses were carried out in the zircons through a sensitive high-resolution ion microprobe (SHRIMP-II, Sato et al., 2014) installed at the CPGeo. Temora 2 was used as a reference for Pb^{206}/U^{238} ages (417 Ma, Black et al., 2004). Data reduction was performed with the SQUID 1.06 software and concordia diagrams were plotted using ISOPLOT 4.

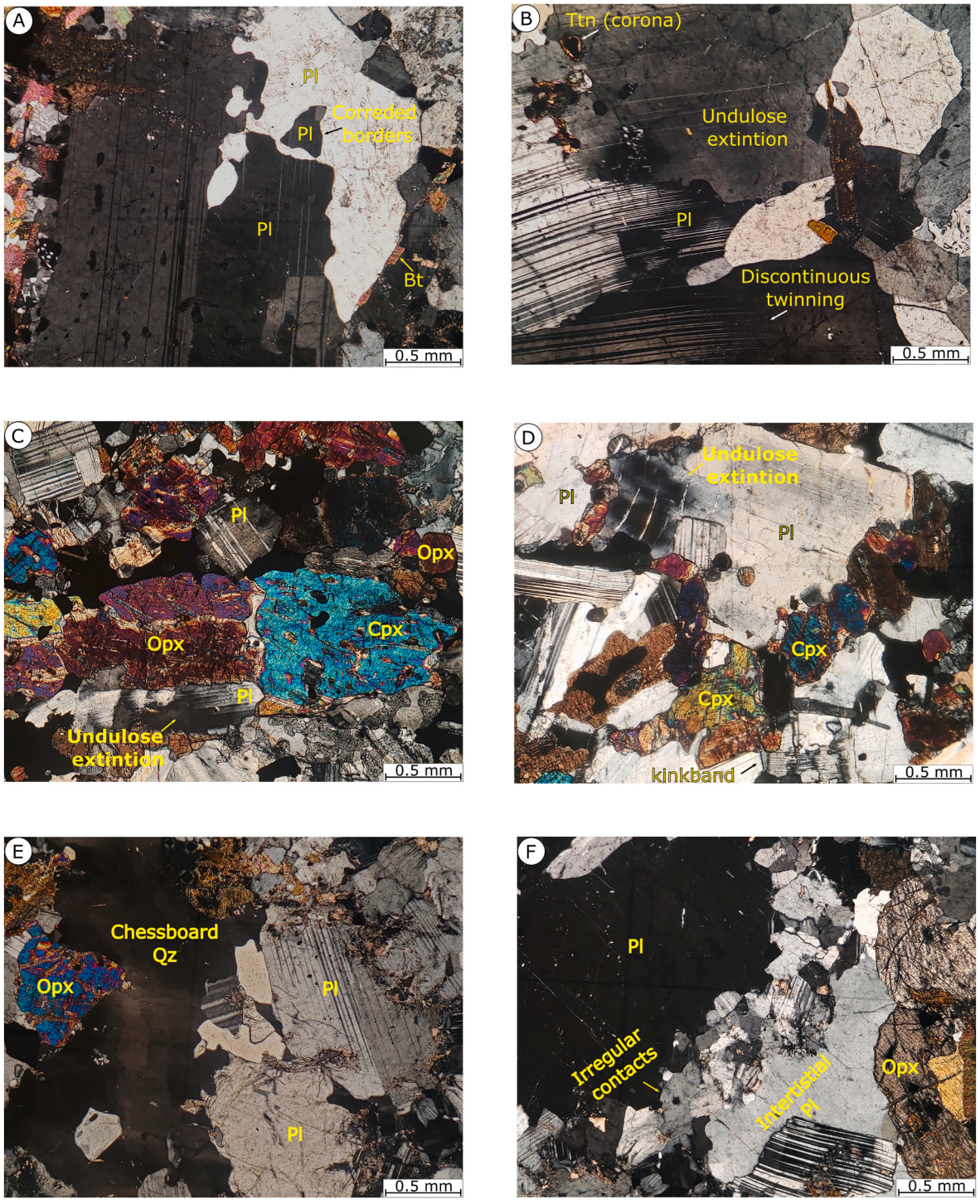

Fig. 7. Thin sections of the dated samples of the VN pluton under polarized light. (A) and (B) correspond to the syenomonzonite, (C) and (D) are the gabbro-norite and (E) and (F) an opx-bearing tonalite. Syenomonzonite and gabbros show evidence of submagmatic deformation (undulose extinction, discontinuous polysynthetic twining and kinkband in plagioclase). Charnockite sample are more intensely deformed, even showing chessboard quartz and irregular contacts of smaller grains (sub grains?) around large plagioclase crystals. Pl – plagioclase, Bt – biotite, Ttn – titanite, Cpx – clinopyroxene, Opx – orthopyroxene, Qz – quartz.

4. Results

4.1. Petrography

The syenomonzonite is a gray colored rock with a fine-to-coarse grained serial inequigranular matrix (0.05–5.5 mm) mostly composed of xenomorphic grains, while the porphyritic texture is given by the phenocrystals (up to 3 cm) of K-feldspar. The major phases are K-feldspar (orthoclase), plagioclase, biotite, amphibole (hornblende), opaque and quartz. While the accessory phase is mainly fine-grained (0.050–0.075 mm) crystals of apatite, zircon (mostly randomly distributed in the matrix of the rock, but are frequently found included in large orthoclase grains), sericite (secondary phase) and titanite. The latter usually occurs as reaction coronas around opaque minerals when in contact with plagioclase or amphibole. The primary grains of quartz show undulose extinction however, it is also possible to observe the formation of myrmekite intergrown in plagioclase when in contact with the perthitic orthoclase. The thin-section displays signs of submagmatic deformation, such as (i) corroded plagioclase borders (Fig. 7A); (ii) curved, sometimes discontinuous, polysynthetic twinning (Fig. 7B) and (iii) strong undulose extinction in plagioclase crystals (Fig. 7B).

The gabbro (Fig. 7C) is a black-to-dark gray colored rock with hydiopiomorphic serial inequigranular (0.05–5.5 mm) matrix and porphyritic texture of plagioclase phenocrystals (1 cm). The trachytoid texture is also displayed by the relevant orientation of tabular plagioclase and pyroxene prisms. The major phases are plagioclase, clinopyroxene, orthopyroxene, opaque, biotite and apatite. The accessory phase is basically composed of fine crystals (<0.075 mm) of sericite (secondary) and zircon which is rare and included in the biotite, without the formation of pleochroic halos. Orthopyroxenes show pleochroism in pinkish second order hues and late first order yellow-pink interference colors in polarized light (PL), typically common in the hypersthene series. However, some orthopyroxenes crystals are recognized as enstatite due to their lack of pleochroism and first-order gray interference colors in PL. The plagioclase displays signs of deformational microstructures, although of inconclusive nature, such as undulating extinction and/or discontinuous polysynthetic kinkband (Fig. 7D) usually in smaller grains.

The charnockite (mainly orthopyroxene-tonalite) is grayish green colored rock with very fine-to-coarse (0.05–7 mm) xenomorphic serial inequigranular texture. The major phases are plagioclase, orthopyroxene, quartz, clinopyroxene, biotite and opaque. The accessory phase is composed by fine grained crystals (<0.05 mm) of zircon and apatite. The zircon grains we observe here are rare to be found in the thin sections, but when present they are mostly prismatic and included in plagioclase or in contact with orthopyroxene grains. The rock has outstanding evidence of solid-state deformation such as: (i) chessboard undulose (Fig. 7E), (ii) strong undulose (Fig. 7F) and/or (iii) kinkband plagioclase, extinction quartz. The coarse pyroxene grains (>3 mm) are usually anhedral and fractured, being possible to observe portions with clusters of small broken mafic grains.

It is important to highlight in all the described rocks the distribution of opaque minerals, where a duality of behavior is observed: (i) the coarser anhedral opaque grains (0.05–0.5 mm) are usually in contact with mafic minerals, filling the spaces between them. On the other hand, (ii) the finer crystals (<0.005 mm) of opaques usually occur as inclusions in poikilitic texture of the pyroxene crystals (more rarely in biotite) which are usually equidimensional rounded or even elongated in the prismatic (elongation in the case of biotite) direction of the mafic crystal.

4.2. U-Pb isotopic dating

For clarity, isotopic data of all measurements are shown in a Supplementary file. Zircon populations will be described for the three geological units evaluated in this paper.

Zircons from the syenomonzonite (n = 14) are mostly euhedral to subhedral, light brown and translucent crystals, with medium to low luminescence (Fig. 8). Inclusions are absent and fractures are rare. Most of these grains have a width to length ratio of 1:3 (although 3 grains have a 1:5 ratio), showing little edge smoothing. Oscillatory zoning occurs in four grains. Mean Th/U ratio for this population is 1.93 ± 0.62. Common Pb with values always lower than 5%, so all of them were used in the calculation of a concordant age of 496.9 ± 4.2 Ma (MSWD = 0.0019) (Fig. 9A).

Zircons from the gabbronorite (n = 14) are anhedral to subhedral, rounded, colorless and translucent crystals (Fig. 8). They have no inclusions and show medium to low luminescence. Oscillatory zoning occurs in just a few of these grains, but most of the zoning does not clearly follow a growing trend (the luminescence of an internal zone is not symmetrical). In few grains, overgrowth of structureless domains of higher luminescence appears at the borders. Mean Th/U ratio for this population is 1.65 ± 0.27. Similarly, to the zircons from the syenomonzonite, common Pb values were below 5%, so all of grains were used in the calculation of a concordant age (Fig. 9B) of 500.6 ± 3.7 Ma (MSWD = 0.0290).

Zircons from the charnockite (opx-tonalite) yield a more complex data when compared to the other units that we have dated in this study (Fig. 8). All grains have common Pb < 5%. Except for a single grain with well-preserved edges, all grains have smooth edges and subhedral shapes (Fig. 8). They are mostly colorless and translucent, some of them showing inclusions of opaque acicular phases. Analysis allowed to separate two zircon sub-populations. The first population (named 'a'; n = 7) has low to mid luminescence, with a well-marked oscillatory zoning and absence of younger unstructured domain growth (at the borders). Mean Th/U ratio for this sub-population is 0.59 ± 0.15. The second sub-population (named 'b'; n = 17) is in some aspects very similar to population 'a', except for the presence of unstructured domain growth at the borders. These grains have low luminescent cores and high luminescent borders, with the transgression of older zones occurring eventually. These zircons with reworked borders do not show differences on the Th/U ratios in rims and cores (mean = 1.65 ± 0.27). The data acquired from these two zircon populations follow the concordia (Fig. 9C), and delimit two main age groups: Group I for sub-population 'a' and by zircon cores from population 'b' (n = 14, 624.0 ± 3.1 Ma, MSWD = 0.116, Fig. 9D), and Group II for high luminescent rims of sub-population 'b' (n = 6, 483.7 ± 7.4 Ma, MSWD = 0.0003, Fig. 9E). Besides these two concordant ages, four rims of sub-population (b) have ages between 600 and 523 Ma.

5. Discussion

The concordant ages of 496.9 ± 4.2 Ma and 500.6 ± 3.7 Ma obtained for the syenomonzonite and gabbro, respectively, likely represent the crystallization age of the main body of the Venda Nova pluton. These ages place definitively this intrusion in the post-collisional phase of the Araçuaí orogen, as previously suggested on the basis of indirect evidence (other similar reversely zoned plutons from southern AO are dated; magnetic fabric majorly free of regional influence and; a stable thermoremanence resulting in a paleomagnetic pole coherent with the Gondwana APW curve around 500 Ma). Table 2 and Fig. 9F presents an updated compilation of the geochronological data published for post-collisional rocks in the AO. Although the ages are comprised along a 50 Ma long interval, their distribution is typically bimodal, as evidenced by the density accumulation line in Fig. 9F with peaks at 525 Ma and 500 Ma (see also Pedrosa-Soares et al., 2020).

Two groups of concordant ages (as discussed in the previous section) were disclosed for the VN charnockite (opx-quartz-diorites) which may be interpreted in the following ways:

a. Group I ages (sub-population 'a' and zircon cores from population 'b', 624.0 ± 3.1 Ma) indicate the crystallization of charnockites and

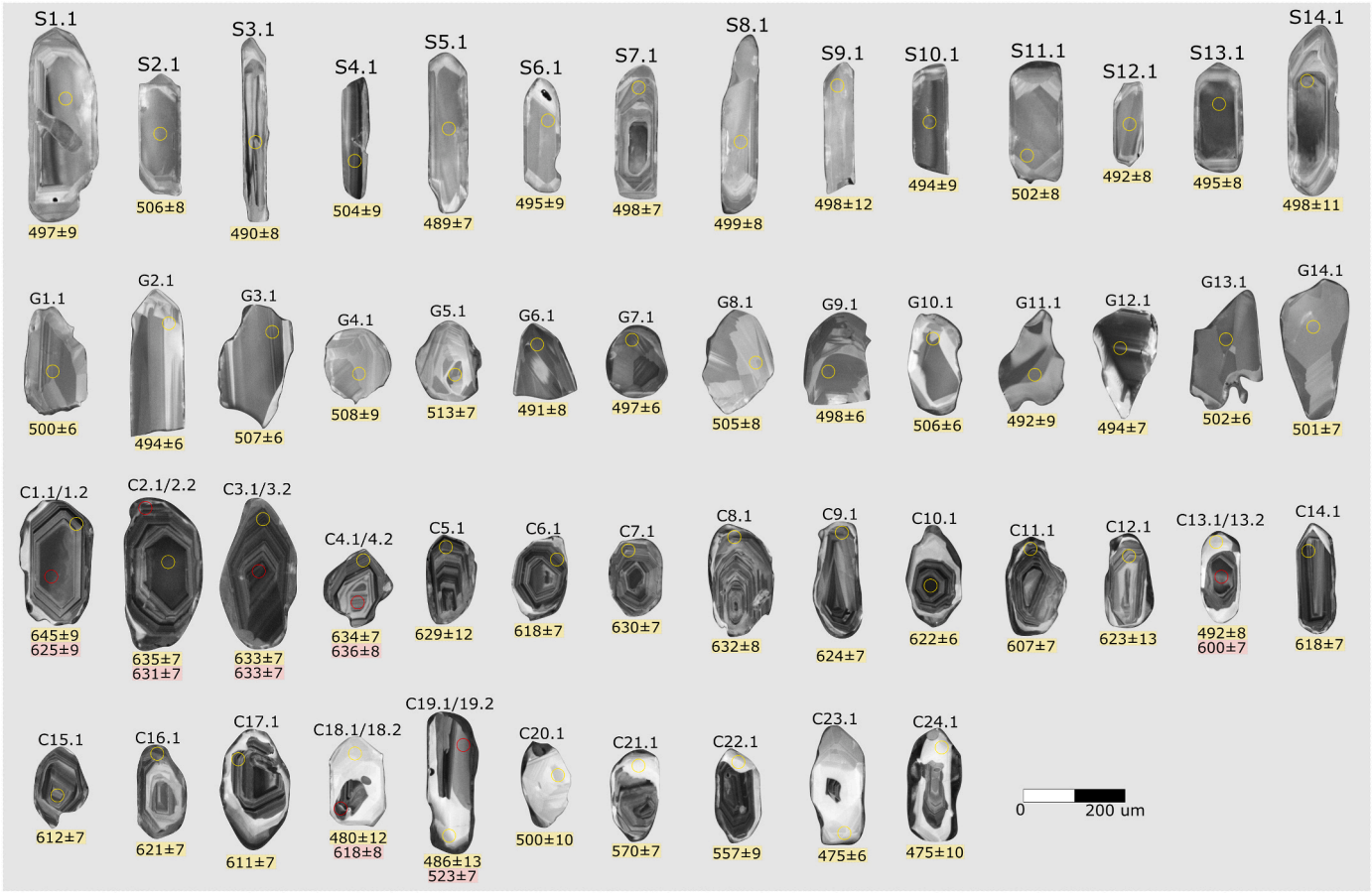

Fig. 8. Cathodoluminescence of zircon grains from syenomonzonite (S), gabbro (G) and charnockite (C) of Venda Nova pluton. Samples are named after the geological unit and the numerical order of grains and spots. Colors are only to differentiate the ages obtain in grains with more than one analyzed spot (yellow spots in the figure correspond to .1, red spots to .2, e.g., C19.1 is the yellow spot of the 19th zircon grain from the charnockite).

Group II ages (rims of sub-population 'b', 483.7 ± 7.4 Ma) represent a resetting during the intrusion of the syenomonzonite and gabbro;

b. Group I ages are from inherited zircons. If so, from which rocks?

Concerning hypothesis (a), an important observation is that few zircons dated at around 500 Ma were found in the charnockite, and the spots were made where luminescence was stronger (Fig. 8). The other zircons all have similar characteristics, including older low-to-mid luminous cores and more strongly luminescent younger rims (when present). If these charnockites are indeed much older than syenomonzonites and gabbros, the sub-solidus ductile deformation described for the charnockitic rocks by Mendes and De Campos (2012), e.g. grain boundary migration, bending of cleavage planes in plagioclase, kinking or folding in biotite and strong undulose extinction, would be better explained by a longer evolutional and deformational history for these rocks. These intense sub-solidus deformation features were also observed in the opx-tonalite sample dated in this work since chessboard quartz (Fig. 7E) is a characteristic high-temperature (>550–600 °C) deformation structure (Kruhl, 1996). Downward flow of previous intruded charnockites induced by diapiric emplacement of the syenomonzonites and gabbros could explain such features.

VN charnockites are less enriched in LREE and HREE than other pre- and post-collisional charnockites, so this comparison is not conclusive in supporting hypothesis (a). However, G5-charnockites are more strongly enriched in Ba than VN charnockites, the latter more enriched in Sr and less differentiated than most of the opx-bearing rocks of the AO. Although not conclusive, the higher anisotropy degrees observed in the charnockite rocks of VN (even when compared with syenomonzonites in the border of the pluton) is also an indication of a "more structured" fabric formed by the alignment of paramagnetic and ferromagnetic (*l.s*) minerals, which agrees with the deformation features observed in macro (see Bellon et al., 2021) and microscale (revisit section 4.1).

On the other hand, in hypothesis (b) these charnockites would be post-collisional as they have been considered for decades of studies, even without geochronological data. If this hypothesis is correct then the older (624 Ma) dated zircons have to be inherited from other rocks in the VN vicinity. Detrital zircons from the Nova Venécia group (the major paraderived country rock VN) show a variety of ages (from 590 to 2124 Ma, Gradim et al., 2014), so it is unlikely that only part of these zircon populations would be selectively inherited by the charnockites (since we have dated all the zircons collected from the separation procedure). Other batholiths in the vicinity of VN are younger than Group I ages. For example, the metagabbronorite from the Serra do Valentim pluton (east from the Muniz Freire batholith) shows a U-Pb, zircon concordant age of 605 ± 8 Ma (Tedeschi et al., 2016), i.e., ca. 20 Ma younger than Group I ages (even if there is a margin for error in the interpretation for data, this is a substantial span of time). The Muniz Freire batholith (a country rock of the VN from the Rio Doce arc) was dated at 588.0 ± 4 Ma (LA-ICP-MS, U-Pb in 25 zircon grains; Pedrosa-Soares et al., 2011), ca. 35 Ma younger than Group I ages. Recently, however, Teixeira et al. (2020) reported a concordant age of 641 ± 5 Ma (U-Pb in zircons) for the Muniz-Freire batholith (also referred as Estrela orthogneiss) located 50 km south of VN, which was interpreted as its crystallization age. Gouvêa et al. (2020) have also reported magmatic pulses dated around 600 Ma (U-Pb in zircon) for pre-collisional near the Estrela orthogneiss. The occurrence of inherited zircons with ages close to Group I is reported in other

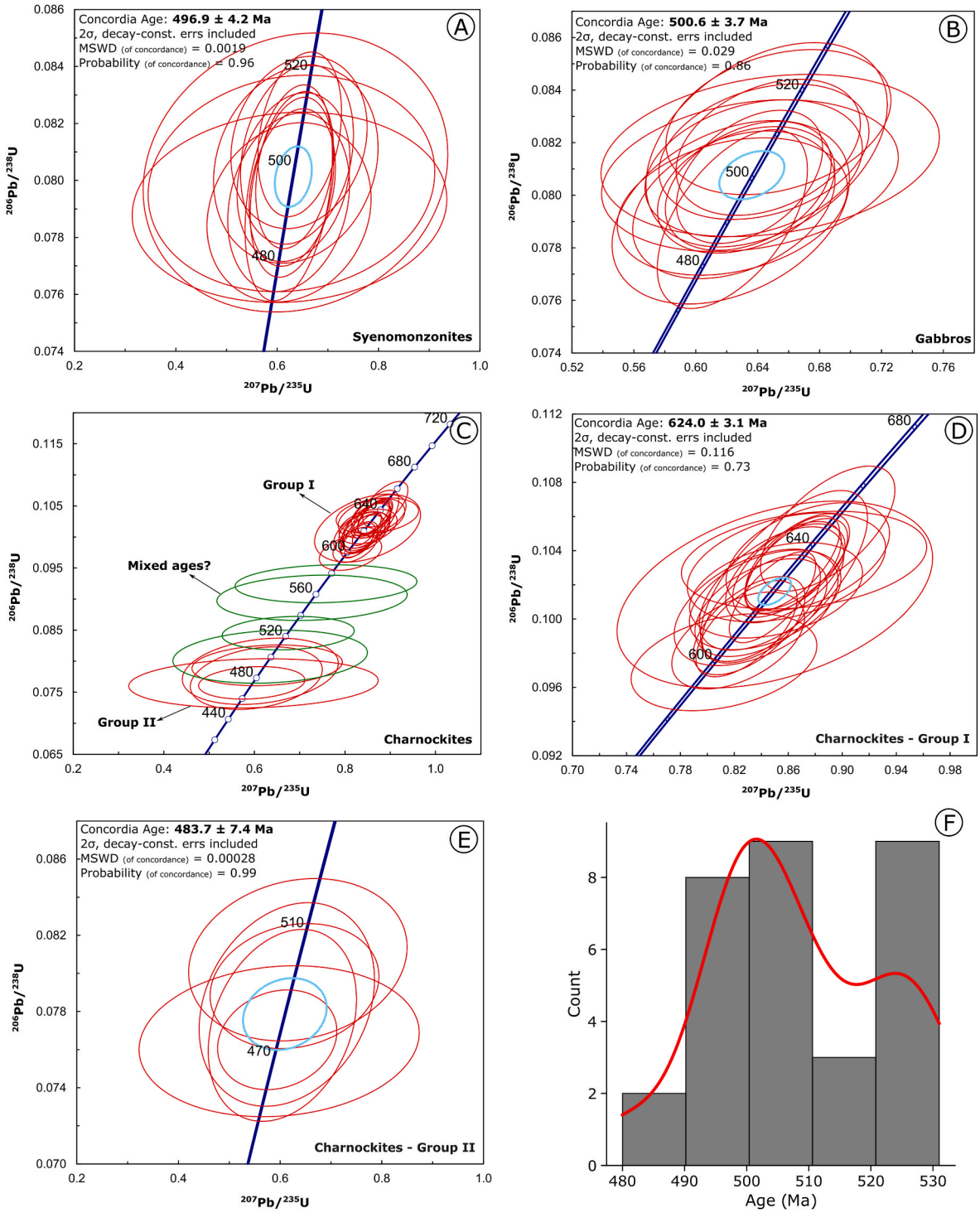

Fig. 9. (A–E) Concordia diagrams and mean rock ages for Venda Nova magmatic facies. (F) Histogram and density accumulation line (in red) for all G5 ages define two major peaks at around 500 Ma and 525 Ma. References used in (F) are listed in Table 2.

post-collisional rocks by Araujo et al. (2020). Rocks from the Muniz-Freire batholith would be the most probable candidate as the source of zircon grains if we consider hypothesis (b) as the correct one, although published literature suggests it is younger than Group I ages.

Paleomagnetic data of VN charnockite are coherent with those found in the syenomonzonite and gabbro, which were used to support that all these VN rocks are indeed contemporaneous (Temporim et al., 2021). However, thermal diffusion of younger syenomonzonite and gabbro could have completely remagnetized the charnockites, which would result in similar characteristic remanent magnetization directions for all these rocks despite any initial gap in their magmatic ages. Therefore, the paleomagnetic data cannot be decisive to define the age of VN charnockites.

Bellon et al. (2021) endorsed a ductile emplacement mechanism model for the VN, where the charnockitic and noritic magmas of the western ring were first emplaced being later intruded by the syenomonzonites and gabbros. To explain the genesis of these VN charnockites, Mendes & De Campos (2012) proposed that these rocks were a

Table 2
Compilation of crystallization ages of post-collisional (G5) intrusions of the AO.

Reference	Unit[a]	Lithotype	Method	System	Age	Uncertainty
Söllner et al. (2000)	Mimoso do Sul (ES)	Granite	ID-TIMS	Concordia age (Zircon)	480	4
Aranda et al. (2020)	Afonso Cláudio (ES)	Quartz-Monzonite	LA-ICP-MS	Concordia age (Zircon)	480.9	3.2
Söllner et al. (2000)	Mimoso do Sul (ES)	Monzosyenite	ID-TIMS	Concordia age (Zircon)	495	5
Aranda et al. (2020)	Afonso Cláudio (ES)	Monzogabbro	LA-ICP-MS	Concordia age (Zircon)	496.5	3.6
Mendes et al. (2005)	Várzea Alegre (ES)	Charnockite	ID-TIMS	Upper intercept (Zircon)	498	5
Temporim et al. (2020)	Santa Angélica (ES)	Gabbro	SHRIMP II	Concordia age (Zircon)	498	5
Mello (2000)	Maciço Intrusivo Aimorés (ES)	Monzo-Granodiorite	LA-ICP-MS	Concordia age (Zircon)	498	35.6
Mello (2000)	Maciço Intrusivo Aimorés (ES)	Charnockite	LA-ICP-MS	Concordia age (Zircon)	498	35.6
Xavier (2017)	Padre Paraíso (MG)	Charnockite	LA-ICP-MS	Concordia age (Zircon)	498	2.4
Belém (2014)	Dique João Neiva (ES)	Gabbro-norite	SHRIMP	Concordia age (Zircon)	498	16
Xavier (2017)	Caladão (MG)	Granite	LA-ICP-MS	Concordia age (Zircon)	500.7	1.5
Serrano et al. (2018)	Medina (MG)	Syenogranite	LA-ICP-MS	Concordia age (Zircon)	501	2
Baltazar et al. (2010)	Maciço Intrusivo Aimorés (MG)	Charnockite	LA-ICP-MS	Concordia age (Zircon)	502	?
Xavier (2017)	Padre Paraíso (MG)	Charnockite	LA-ICP-MS	Concordia age (Zircon)	502.7	1.9
De Campos et al. (2016)	Cotaché (ES)	Granite	LA-ICP-MS	Concordia age (Zircon)	504	3
Araujo et al. (2020)	Vitória (ES)	Tonalite	LA-ICP-MS	Concordia age (Zircon)	505	1
Temporim et al. (2020)	Santa Angélica (ES)	Granite	SHRIMP II	Concordia age (Zircon)	506	3
Medeiros (1999)	Várzea Alegre (ES)	Granite	Rb/Sr	Whole Rock	507	33
Belém (2014)	Dique Pendanga (ES)	Olivine-basalt	SHRIMP II	Concordia age (Zircon)	509	16
Xavier (2017)	Caladão (MG)	Granite	LA-ICP-MS	Concordia age (Zircon)	512.1	1.5
Söllner et al. (2000)	Santa Angélica (ES)	Granite	ID-TIMS	Upper intercept (Zircon)	513	8
Baltazar et al. (2010)	Maciço Intrusivo Aimores (MG)	Charnockite	LA-ICP-MS	Concordia age (Zircon)	513	?
Araujo et al. (2020)	Aracê - Pedra Azul (ES)	Granite	LA-ICP-MS	Concordia age (Zircon)	523	2
De Campos et al. (2016)	Pedra do Elefante (ES)	Charnockite	LA-ICP-MS	Concordia age (Zircon)	524	3.2
Gradim et al. (2014)	Barra do São Francisco (ES)	Charnockite	LA-ICP-MS	Upper intercept (Zircon)	524	3.2
Belém (2014)	São Gabriel da Baunilha	Norite	SHRIMP II	Concordia age (Zircon)	524	7
Belém (2014)	Dique Alto Santa Maria (ES)	Enderbitic norite	SHRIMP II	Concordia age (Zircon)	525	10
Gonçalves et al. (2016)	Fronteira dos Vales (MG)	Granodiorite	LA-ICP-MS	Concordia age (Zircon)	526	5
Araujo et al. (2020)	Mestre Álvaro (ES)	Granite	LA-ICP-MS	Concordia age (Zircon)	527	2
De Campos et al. (2016)	Pedra do Elefante (ES)	Granite	LA-ICP-MS	Concordia age (Zircon)	531	34
Teixeira et al. (2020)	Alto Chapéu (ES)	Granite	LA-ICP-MS	Concordia age (Zircon)	531	4

Note:
[a] Geological units are followed by the abbreviation of their correspondent location in a Brazilian State.

product of fractional crystallization either (i) from an anhydrous magma of calc-alkaline composition or (ii) from a tholeiitic magma that would induce partial melting on the crust (after mixing with tholeiitic magma) and such a process could generate calc-alkaline magma batches. These magmas should have intruded along the dextral transpressional shear zones that impose structural control on the pre-to-syntectonic rocks of southern AO (Alkmim et al., 2006). However, if charnockites are the country rocks of syenomonzonites and gabbros from a pre-collisional orogenic stage, then the evolutional history should also be different.

Novo et al. (2010) considered the pre-collisional charnockitic rocks from the Divino Suite (discussed in section 2.3) as derived from a magmatic arc related to an active margin that received important inputs from deep crustal Paleoproterozoic sources, interpreting them as the root of such magmatic arc. In this collisional scenario, north-to-south pre-to-early collisional rocks would form a corridor marking what has been interpreted as a calc-alkaline magmatic arc correspondent to the G1 suite (Pedrosa-Soares et al., 2001; Alkmim et al., 2006; Tedeschi et al., 2016). Charnockites from the border of VN (and by extension the associated norites) would then be part of this orogenic root, which would also agree with calculation of deep pressures and high temperatures performed by Mendes and De Campos (2012).

The intrusion of syenomonzonites and gabbros during a post-collisional stage (together with other magmas from the post-collisional suite) marks a change in the tectonic regime from collisional to extensional. Diapiric rising of syenomonzonites and gabbros and the consequent downward flow of the crust caused by their intrusion should explain why the magnetic fabric of charnockites do not show the regional trend of pre-to-syn-collisional rocks, but dips towards the syenomonzonites and gabbros (Bellon et al., 2021). Besides, the younger U-Pb ages obtained from the luminous borders of two grains in the charnockites (Figs. 8 and 557.0 ± 9 and 570.0 ± 7 Ma) could also be the result of metamorphic reworking of these rocks during the syn-collisional period of AO (although inherited zircons could also have suffered such metamorphic overprint).

6. Final remarks and conclusions

New U-Pb ages are reported for the Venda Nova pluton, a reversely zoned pluton in the Araçuaí orogen. The syenomonzonite sample (internal zone) yielded U-Pb concordant ages of 496.9 ± 4.2 Ma (MSWD = 0.0019) that overlap the age of the gabbroic core (500.6 ± 3.7 Ma, MSWD = 0.0290). These ages agree with the 506 ± 3 Ma and 498 ± 5 Ma ages obtained previously for the Santa Angélica Suite (Temporim et al., 2020) giving support for a mean age around 500 Ma for the key paleomagnetic pole calculated for the VN and Santa Angélica rocks by Temporim et al. (2021).

U-Pb ages for zircons extracted from the charnockite range from 645 ± 9 to 475 ± 10 Ma. Two groups of ages were identified: an older one (n = 14, 624.0 ± 3.1 Ma, MSWD = 0.116), which includes cores and rims of zircons without evidence of border reworking, and a younger one (n = 6, 483.7 ± 7.4 Ma, MSWD = 0.0003) from zircons with luminous rims and older cores. Although it is possible to relate the older ages to inherited zircons of pre-collisional rocks, we prefer to interpret them as crystallization ages of charnockite-norite external ring of VN. The main evidence in favor of that interpretation are: (i) a geochemical signature of VN charnockites that differs from other post-collisional charnockites in the Araçuaí orogen (more metaluminous, less enriched in LILE and HFSE), (ii) higher anisotropy degree compared to other portions of the VN pluton, that (together with microstructural evidence) points towards a magnetic fabric more intensely deformed than other units of the VN, (iii) the presence of sub-solidus deformation (even though concordant with the rest of the border regions of the VN) in the charnockites in contrast to the purely magmatic fabric in most of the pluton and (iv) the lack of zircons containing only ages near 500 Ma. VN charnockites could be, therefore, part of the orogenic root of the AO in a pre-collisional setting.

This is the first reported example of a structure with borders that can be far older than the inner units in a reversely zoned pluton of the AO.

CRediT authorship contribution statement

U.D. Bellon: Writing – original draft, Visualization, Methodology, Investigation, Formal analysis, Conceptualization. **G.F. Souza Junior:** Visualization, Investigation, Formal analysis, Conceptualization. **F.A. Temporim:** Visualization, Formal analysis, Data curation. **M.S. D'Agrella-Filho:** Writing – review & editing, Supervision, Resources, Methodology, Investigation, Data curation. **R.I.F. Trindade:** Writing – review & editing, Supervision, Resources, Funding acquisition, Conceptualization.

Declaration of competing interest

The authors declare that they have no known competing financial interests or personal relationships that could have appeared to influence the work reported in this paper.

Data availability

Data will be made available on request.

Acknowledgments

This study was supported by FAPESP (grant 2016/06114–6). We also would like to thank the support provided by the technicians from the Research Center in Geochronology and Isotopic Geochemistry (CPGeo) at the University of São Paulo. We especially thank Prof. Dr. Julio Mendes and another anonymous revisor, their review has certainly improved the quality of this work.

Appendix A. Supplementary data

Supplementary data to this article can be found online at https://doi.org/10.1016/j.jsames.2022.104045.

References

Alkmim, F.F., Marshak, S., Pedrosa-Soares, A.C., Peres, G.G., Cruz, S.C.P., Whittington, A., 2006. Kinematic evolution of the Araçuaí-west Congo orogen in Brazil and Africa: nutcracker tectonics during the Neoproterozoic assembly of Gondwana. Precambrian Res. 149, 43–64. https://doi.org/10.1016/j.precamres.2006.06.007.

Aranda, R.O., Chaves, A.O., Medeiros Júnior, E.B., Venturini Junior, R., 2020. Petrology of the Afonso Cláudio intrusive complex: new insights for the Cambro-Ordovician post-collisional magmatism in the Araçuaí-west Congo orogen, southeast Brazil. J. S. Am. Earth Sci. 98, 102465 https://doi.org/10.1016/j.jsames.2019.102465.

Araujo, Cristina, Pedrosa-Soares, A., Lana, C., Dussin, I., Queiroga, G., Serrano, P., Medeiros-Júnior, E., 2020a. Zircon in emplacement borders of post-collisional plutons compared to country rocks: a study on morphology, internal texture, U–Th–Pb geochronology and Hf isotopes (Araçuaí orogen, SE Brazil). Lithos 352–353. https://doi.org/10.1016/j.lithos.2019.105252.

Araujo, C., Pedrosa-Soares, A., Lana, C., Dussin, I., Queiroga, G., Serrano, P., Medeiros-Júnior, E., 2020b. Zircon in emplacement borders of post-collisional plutons compared to country rocks: a study on morphology, internal texture, U–Th–Pb geochronology and Hf isotopes (Araçuaí orogen, SE Brazil). Lithos 352–353. https://doi.org/10.1016/j.lithos.2019.105252.

Assumpção, M., Bianchi, M., Julià, J., Dias, F.L., Sand França, G., Nascimento, R., Drouet, S., Pavão, C.G., Albuquerque, D.F., Lopes, A.E.V., 2013. Crustal thickness map of Brazil: data compilation and main features. J. S. Am. Earth Sci. 43, 74–85. https://doi.org/10.1016/j.jsames.2012.12.009.

Baltazar, O.F., Zuchetti, M., Oliveira, S.A.M., Scandolara, J., Silva, L.C., 2010. Folha São Gabriel da Palha e Linhares. Belo Horizonte.

Bayer, P., Schmidt-Thomé, R., Weber-Diefenbach, K., Horn, H.A., 1987. Complex concentric granitoid intrusions in the coastal mobile belt, Espírito Santo, Brazil: the Santa Angélica Pluton - an example. Geol. Rundsch. 76, 357–371. https://doi.org/10.1007/BF01821080.

Belém, J., 2014. Geoquímica, Geocronologia E Contexto Geotectônico Do Magmatismo Máfico Associado Ao Feixe De Fraturas Colatina. Universidade Federal de Minas Gerais, Estado Do Espírito Santo.

Bellon, U.D., D'Agrella-Filho, M.S., Temporim, F.A., Souza Junior, G.F., Soares, C.C.V., Amaral, C.A.D., Gouvêa, L.P., Trindade, R.I.F., 2021. Building an inversely zoned post-orogenic intrusion in the Neoproterozoic-Cambrian Araçuaí orogen (Brazil). J. Struct. Geol. 149, 104401 https://doi.org/10.1016/j.jsg.2021.104401.

Black, L.P., Kamo, S.L., Allen, C.M., Davis, D.W., Aleinikoff, J.N., Valley, J.W., Mundil, R., Campbell, I.H., Korsch, R.J., Williams, I.S., Foudoulis, C., 2004. Improved 206Pb/238U microprobe geochronology by the monitoring of a trace-element-related matrix effect; SHRIMP, ID-TIMS, ELA-ICP-MS and oxygen isotope documentation for a series of zircon standards. Chem. Geol. 205, 115–140. https://doi.org/10.1016/j.chemgeo.2004.01.003.

Borradaile, G.J., 1991. Correlation of strain with anisotropy of magnetic susceptibility (AMS). Pure Appl. Geophys. 135, 15–29. https://doi.org/10.1007/BF00877006.

Borradaile, G.J., Henry, B., 1997. Tectonic applications of magnetic susceptibility and its anisotropy. Earth Sci. Rev. 42, 49–93. https://doi.org/10.1016/S0012-8252(96)00044-X.

Bouchez, J.L., 1997. Granite is never isotropic: an introduction to AMS studies of granitic rocks. In: Bouchez, J.L., Hutton, D.H.W., Stephens, W.E. (Eds.), Studies of Granitic Rocks Granite : from Segregation of Melt to Emplacement Fabrics, vol. 45. Kluwer Academic Publishers. https://doi.org/10.1007/978-94-017-1717-5_6.

Boynton, W.V., 1983. Cosmochemistry of the rare earth elements: meteorite studies. In: Rare Earth Element Geochemistry. Elsevier B.V., pp. 63–114. https://doi.org/10.1016/b978-0-444-42148-7.50008-3

Cavalcante, C., Fossen, H., Paes, R., Almeida, D., Helena, M., Hollanda, B.M., Egydio-silva, M., 2019. Reviewing the puzzling intracontinental termination of the Araçuaí-West Congo orogenic belt and its implications for orogenic development. Precambrian Res. 322, 85–98 https://doi.org/https://doi.org/10.1016/j.precamres.2018.12.025.

Cavalcante, C., Hollanda, M., Vauchez, A., Kawata, M., 2018. How long can the middle crust remain partially molten during orogeny. Geology 46, 839–842.

Caxito, F.A., Hartmann, L.A., Heilbron, M., Pedrosa-Soares, A.C., Bruno, H., Basei, M.A.S., Chemale, F., 2022. Multi-proxy evidence for subduction of the Neoproterozoic Adamastor ocean and Wilson cycle tectonics in the south Atlantic Brasiliano orogenic system of western Gondwana. Precambrian Res. 376 https://doi.org/10.1016/j.precamres.2022.106678.

CPRM, 2010. Projeto Aerogeofísico Espírito Santo (1093). Rio de Janeiro.

Da Silva, L.C., Pedrosa-Soares, A.C., Armstrong, R., Noce, C.M., 2011. Determinando a Duração do Período Colisional do Orógeno Araçuaí Com Base Em Geocronologia U-Pb de Alta Resolução Em Zircão: Uma Contribuição Para a História Da Amalgamação do Gondwana Ocidental. Geonomos 19, 180–197. https://doi.org/10.18285/geonomos.v19i2.53.

De Campos, C.P., de Medeiros, S.R., Mendes, J.C., Pedrosa-Soares, A.C., Dussin, I., Ludka, I.P., Dantas, E.L., 2016. Cambro-ordovician magmatism in the Araçuaí belt (SE Brazil): snapshots from a post-collisional event. J. S. Am. Earth Sci. 68, 248–268 https://doi.org/https://doi.org/10.1016/j.jsames.2015.11.016.

De Campos, C.P., Mendes, J.C., Ludka, I.P., de Medeiros, S.R., de Moura, J.C., Wallfass, C., 2004. A review of the Brasiliano magmatism in southern Espírito Santo, Brazil, with emphasis on post-collisional magmatism. J. Virtual Explor. 17, 1–44. https://doi.org/10.3809/jvirtex.2004.00106.

Egydio-Silva, M., Vauchez, A., Fossen, H., Gonçalves Cavalcante, G.C., Xavier, B.C., 2018. Connecting the Araçuaí and Ribeira belts (SE – Brazil): progressive transition from contractional to transpressive strain regime during the Brasiliano orogeny. J. S. Am. Earth Sci. 86, 127–139. https://doi.org/10.1016/j.jsames.2018.06.005.

El Bouseily, A.M., El Sokkary, A.A., 1975. The relation between Rb, Ba and Sr in granitic rocks. Chem. Geol. 16, 207–219. https://doi.org/10.1016/0009-2541(75)90029-7.

Fossen, H., Cavalcante, C., Konopásek, J., Meira, V.T., de Almeida, R.P., Hollanda, M.H.B.M., Trompette, R., 2020. A critical discussion of the subduction-collision model for the Neoproterozoic Araçuaí-West Congo orogen. Precambrian Res. 343 https://doi.org/10.1016/j.precamres.2020.105715.

Fossen, H., Cavalcante, C.G., de Almeida, R.P., 2017. Hot versus cold orogenic behavior : comparing. Tectonics 36, 2159–2178. https://doi.org/10.1002/2017TC004743.

Frost, B.R., Barnes, C.G., Collins, W.J., Arculus, R.J., Ellis, D.J., Frost, C.D., 2001. A geochemical classification for granitic rocks. J. Petrol. 42, 2033–2048. https://doi.org/10.1093/petrology/42.11.2033.

Gonçalves, L., Alkmim, F.F., Pedrosa-Soares, A.C., Dussin, I.A., Valeriano, C. de M., Lana, C., Tedeschi, M., 2016. Granites of the intracontinental termination of a magmatic arc: an example from the Ediacaran Araçuaí orogen, southeastern Brazil. Gondwana Res. 36, 439–458. https://doi.org/10.1016/j.gr.2015.07.015.

Gonçalves, L., Farina, F., Lana, C., Pedrosa-Soares, A.C., Alkmim, F., Nalini, H.A., 2014. New U–Pb ages and lithochemical attributes of the Ediacaran Rio Doce magmatic arc, Araçuaí confined orogen, southeastern Brazil. J. S. Am. Earth Sci. 52, 129–148. https://doi.org/10.1016/j.jsames.2014.02.008.

Gouvêa, L.P., de Medeiros, S.R., Mendes, J.C., Soares, C., Marques, R., Melo, M., 2020. Magmatic activity period and estimation of P-T metamorphic conditions of pre-collisional opx-metatonalite from Araçuaí-Ribeira orogens boundary, SE Brazil. J. S. Am. Earth Sci. 99, 102506 https://doi.org/10.1016/j.jsames.2020.102506.

Gradim, C., Roncato, J., Pedrosa-Soares, A.C., Cordani, U., Dussin, I., Alkmim, F.F., Queiroga, G., Jacobsohn, T., Da Silva, L.C., Babinski, M., 2014. The hot back-arc zone of the Araçuaí orogen, eastern Brazil: from sedimentation to granite generation. Braz. J. Geol. 44, 155–180. https://doi.org/10.5327/Z2317-4889201400010012.

Horn, H.A., Weber-Diefenbach, W., 1987. Geochemical and genetic studies of three inverse zoned intrusive bodies of both alkaline and calc-alkaline composition in the Ribeira Mobile Belt (Espírito Santo, Brazil). Rev. Bras. Geociencias 17, 488–497.

Irvine, T.N., Baragar, W.R.A., 1971. A guide to the chemical classification of the common volcanic rocks. Can. J. Earth Sci. 8, 523–548. https://doi.org/10.1139/e71-055.

Jelinek, V., 1981. Characterization of the magnetic fabric of rocks. Tectonophysics 79, 63–67. https://doi.org/10.1016/0040-1951(81)90110-4.

Jelinek, V., 1977. The statistical theory of measuring anisotropy of magnetic susceptibility of rocks and its application. Geofyzika 29, 1–87.

Jelínek, V., 1978. Statistical processing of anisotropy of magnetic susceptibility measured on groups of specimens. Studia Geophys. Geod. 22, 50–62. https://doi.org/10.1007/BF01613632.

Konopásek, J., Cavalcante, C., Fossen, H., Janoušek, V., 2020. Adamastor – an ocean that never existed? Earth Sci. Rev. 205, 103201 https://doi.org/10.1016/j.earscirev.2020.103201.

Kruhl, J.H., 1996. Prism- and basal-plane parallel subgrain boundaries in quartz: a microstructural geothermobarometer. J. Metamorph. Geol. 14, 581–589. https://doi.org/10.1046/j.1525-1314.1996.00413.x.

Ludka, I.P., Wiedemann-Leonardos, C.M., 2000. Further signs of an enriched mantle source under the Neoproterozoic Araçuaí-Ribeira mobile belt. Rev. Bras. Geociencias 30, 95–98. https://doi.org/10.25249/0375-7536.2000301095098.

Ludka, I.P., Wiedemann, C.M., Töpfner, C., 1998. On the origin of incompatible element enrichment in the Venda Nova pluton, State of Espirito Santo, southeast Brazil. J. S. Am. Earth Sci. 11, 473–486. https://doi.org/10.1016/S0895-9811(98)00028-5.

Medeiros, S.R., 1999. Estudo mineralógico, petrológico, geoquímico e isotópico do complexo intrusivo de Várzea Alegre – ES. Universidade Federal do Rio de Janeiro.

Medeiros, S.R., Wiedemann-Leonardos, C.M., Vriend, S., 2001. Evidence of mingling between contrasting magmas in a deep plutonic environment: the example of Várzea Alegre, in the Ribeira Mobile Belt, Espírito Santo, Brazil. An Acad. Bras Ciências 73, 99–119. https://doi.org/10.1590/S0001-37652001000100009.

Medeiros, S.R., Wiedemann, C.M., Mendes, J.C., 2000. Post-collisional multistage magmatism in the Ribeira mobile belt: geochemical and isotopic study of the Varzea Alegre intrusive complex, Espírito Santo, Brazil. Rev. Bras. Geociencias 31, 30–34.

Melo, M.G., Lana, C., Stevens, G., Hartwig, M.E., Pimenta, M., Nalini, H.A., 2020. Deciphering the source of multiple U–Pb ages and complex Hf isotope composition in zircon from post-collisional charnockite-granite associations from the Araçuaí orogen (southeastern Brazil). J. S. Am. Earth Sci. 103, 102792 https://doi.org/10.1016/j.jsames.2020.102792.

Mello, F.M., 2000. Litogeoquímica e química mineral do maciço charnockítico Aimorés-MG. Universidade de São Paulo.

Mendes, J.C., De Campos, C.M.P., 2012. Norite and charnockites from the Venda Nova Pluton, SE Brazil: intensive parameters and some petrogenetic constraints. Geosci. Front. 3, 789–800 https://doi.org/https://doi.org/10.1016/j.gsf.2012.05.009.

Mendes, J.C., de Medeiros, S.R., McReath, I., de Campos, C.M.P., 2005. Cambro-Ordovician magmatism in SE Brazil: U-Pb and Rb-Sr ages, combined with Sr and Nd isotopic data of Charnockitic rocks from the Varzea Alegre Complex. Gondwana Res. 8, 337–345 https://doi.org/https://doi.org/10.1016/S1342-937X(05)71139-4.

Mendes, J.C., McReath, I., Wiedemann, C.M., Figueiredo, M.C.H., 1997. Charnockitóides do maciço de várzea alegre: um novo exemplo do magmatismo cálcio-alcalino de alto-K no arco magmático do Espírito Santo. Rev. Bras. Geociencias 27, 13–24.

Novo, T.A., Pedrosa Soares, A.C., Noce, C.M., Alkmim, F.F., Dussin, I.A., 2010. Rochas charnockíticas do sudeste de Minas Gerais:: a raiz granulítica do arco magmático do Orógeno Araçuaí. Rev. Bras. Geociencias 40.

Pedrosa-Soares, A.C., Castañeda, C., Queiroga, G., Gradim, C., Belém, J., Roncato, J., Novo, T., Dias, P., Gradim, D., Medeiros, S., Jacobsohn, T., Babinski, M., Vieira, V., 2006. Magmatismo e tectônica do Orógeno Araçuaí no extremo leste de Minas e norte do Espirito Santo (18°-19°S, 41°-40°30′W). Geonomos 14, 97–111. https://doi.org/10.18285/geonomos.v14i2.114.

Pedrosa-Soares, A.C., De Campos, C.P., Noce, C., Silva, L.C., Novo, T., Roncato, J., Medeiros, S., Castañeda, C., Queiroga, G., Dantas, E., Dussin, I., Alkmim, F., 2011. Late Neoproterozoic – Cambrian granitic magmatism in the Araçuaí orogen (Brazil), the eastern Brazilian pegmatite province and related mineral resources. Geol. Soc. Lond. Spec. Publ. 350, 25–51 https://doi.org/https://doi.org/10.1144/SP350.3.

Pedrosa-Soares, A.C., Deluca, C., Araujo, C.S., Gradim, C.S., Lana, C.C., Dussin, I., Silva, L.C., Babinski, M., 2020. O Orógeno Araçuaí à luz da Geocronologia: um tributo a Umberto Cordani. In: Bartorelli, A., Teixeira, W., Brito Neves, B.B. (Eds.), Geocronologia e Evolução Tectônica Do Continente Sul-Americano: A Contribuição de Umberto Giuseppe Cordani. Solaris Edições Culturais, São Paulo, pp. 250–272.

Pedrosa-soares, A.C., Noce, C.M., Alkmim, F.F., Carlos, L., Babinski, M., Cordani, U., Castañeda, C., 2007. Orógeno Araçuaí: síntese do conhecimento 30 anos após Almeida 1977. Geonomos 15, 1–16 https://doi.org/https://doi.org/10.18285/geonomos.v15i1.103.

Pedrosa-Soares, A.C., Noce, C.M., Wiedemann, C.M., Pinto, C.P., 2001. The Araçuaí-West-Congo Orogen in Brazil: an overview of a confined orogen formed during Gondwanaland assembly. Precambrian Res. 110, 307–323. https://doi.org/10.1016/S0301-9268(01)00174-7.

Pedrosa-Soares, A.C., Wiedemann-Leonardos, C.M., 2000. Evolution of the Araçuaí belt and its connection to the Ribeira belt , eastern Brazil. In: Cordani, U., Milani, E.J., Thomaz, A., Campos, D.A. (Eds.), Tectônic Evolution of South America. https://doi.org/10.13140/2.1.3802.5928, 265–285.

Peixoto, C.A., Heilbron, M., Ragatky, D., Armstrong, R., Dantas, E., Valeriano, C.M., Simonetti, A., 2017. Tectonic evolution of the Juvenile Tonian Serra da Prata magmatic arc in the Ribeira belt, SE Brazil: implications for early west Gondwana amalgamation. Precambrian Res. 302, 221–254 https://doi.org/https://doi.org/10.1016/j.precamres.2017.09.017.

Petitgirard, S., Vauchez, A., Egydio-Silva, M., Bruguier, O., Camps, P., Monié, P., Babinski, M., Mondou, M., 2009. Conflicting structural and geochronological data from the Ibituruna quartz-syenite (SE Brazil): effect of protracted "hot" orogeny and slow cooling rate? Tectonophysics 477, 174–196. https://doi.org/10.1016/j.tecto.2009.02.039.

Sato, K., Tassinari, C.C.G., Basei, M.A.S., Siga, O., Onoe, A.T., De Souza, M.D., 2014. Sensitive high resolution ion microprobe (SHRIMP IIe/MC) of the Institute of Geosciences of the University of São Paulo, Brazil: analytical method and first results. Geol. Usp. Série Científica 14, 3–18. https://doi.org/10.5327/Z1519-874X201400030001.

Serrano, P., Pedrosa-Soares, A., Medeiros-Júnior, E., Fonte-Boa, T., Araujo, C., Dussin, I., Queiroga, G., Lana, C., 2018. A-type Medina batholith and post-collisional anatexis in the Araçuaí orogen (SE Brazil). Lithos. https://doi.org/10.1016/j.lithos.2018.09.009, 320–321, 515–536.

Schmidt, M.W., 1992. Amphibole composition in tonalite as a function of pressure: an experimental calibration of the Al-in-hornblende barometer. Contrib. Mineral. Petrol. 110, 304–310. https://doi.org/10.1007/BF00310745.

Shand, S.J., 1927. Eruptive rocks: their genesis, composition, classification, and their relation to ore-deposits; with a chapter on meteorites. Nature 120. https://doi.org/10.1038/120872a0, 872–872.

Söllner, F., Lammerer, B., Wiedemann-Leonardos, 2000. Dating the Ribeira mobile belt. Z. Angew. Geol. Sonderheft SH1 245–255.

Souza Junior, G.F., Trindade, R.I.F., Temporim, F.A., Bellon, U.D., Gouvêa, L.P., Soares, C.C., Amaral, C.A.D., Louro, V., 2021. Imaging the roots of a post-collisional pluton: implications for the voluminous Cambrian magmatism in the Araçuaí orogen (Brazil). Tectonophysics 821, 229146. https://doi.org/10.1016/j.tecto.2021.229146.

Tedeschi, M., Novo, T., Pedrosa-Soares, A., Dussin, I., Tassinari, C., Silva, L.C., Gonçalves, L., Alkmim, F., Lana, C., Figueiredo, C., Dantas, E., Medeiros, S., De Campos, C., Corrales, F., Heilbron, M., 2016. The Ediacaran Rio Doce magmatic arc revisited (Araçuaí-Ribeira orogenic system, SE Brazil). J. S. Am. Earth Sci. 68, 167–186 https://doi.org/https://doi.org/10.1016/j.jsames.2015.11.011.

Teixeira, P.A.D., Fernandes, C.M., Mendes, J.C., Medeiros, S.R., Rocha, I.S., 2020. U-PB LA-ICP-MS and geochemical data of the Alto Chapéu Pluton: contributions on bimodal post-collisional magmatism in the Araçuaí belt (SE Brazil). J. S. Am. Earth Sci. 103, 102724 https://doi.org/10.1016/j.jsames.2020.102724.

Temporim, F.A., Bellon, U.D., Domeier, M., Trindade, R.I.F., Agrella-filho, M.S.D., 2021. Constraining the Cambrian drift of Gondwana with new paleomagnetic data from post-collisional plutons of the Araçuaí orogen, SE Brazil. Precambrian Res. 359, 106212 https://doi.org/10.1016/j.precamres.2021.106212.

Temporim, F.A., Trindade, R.I.F., Tohver, E., Soares, C.C., Gouvêa, L.P., Egydio-Silva, M., Amaral, C.A.D., Souza, G.F., 2020. Magnetic fabric and geochronology of a Cambrian "isotropic" pluton in the Neoproterozoic Araçuaí orogen. Tectonics 39, 1–21. https://doi.org/10.1029/2019TC005877.

Wakita, H., Rey, P., Schmitt, R.A., 1971. Abundances of the 14 rare-earth elements and 12 other trace elements in Apollo 12 samples: five igneous and one breccia rocks and four soils. Proc. Lunar Sci. Conf. 2, 1319.

Wiedemann, C.M., Bayer, P., Horn, H., Lammerer, B., Ludka, I.P., Schmidt-Thomé, R.S., Diefenbach, K.W., 1986. Maciços intrusivos do Sul do Espírito Santo e seu contexto regional. Rev. Bras. Geociencias 16, 24–37.

Wiedemann, C.M., De Medeiros, S.R., Ludka, I.P., Mendes, J.C., Costa-de-Moura, J., 2002. Architecture of late orogenic plutons in the Araçuaí-Ribeira fold belt, southeast Brazil. Gondwana Res. 5, 381–399. https://doi.org/10.1016/S1342-937X(05)70730-9.

Xavier, B.C., 2017. Relações Tectônicas no Setor Central da Faixa Araçuaí : Análise Estrutural por ASM e Geocronologia U/Pb e Lu/Hf. Universidade de São Paulo.

Zanon, M.L., Chaves, A.D., Rangel, C.V.G.T., Gaburo, L., Pires, C.R., 2015. Os aspectos geológicos do maciço santa angélica (ES): Uma nova abordagem. Braz. J. Geol. 45, 609–633. https://doi.org/10.1590/2317-4889201520150005.